Tool path compensation strategies for single point incremental sheet forming using Multivariate Adaptive Regression Splines

Amar Kumar Behera*, Johan Verbert, Bert Lauwers, Joost R. Duflou

Katholieke Universiteit Leuven, Department of Mechanical Engineering, Celestijnenlaan 300B, B-3001 Leuven, Belgium

Abstract

Single point incremental sheet forming is an emerging sheet metal prototyping process that can produce parts without requiring dedicated tooling per part geometry. One of the major issues with the process concerns the achievable accuracy of parts, which depends on the type of features present in the part and their interactions with one another. In this study, the authors propose a solution to improve the accuracy by using Multivariate Adaptive Regression Splines (MARS) as an error prediction tool to generate continuous error response surfaces for individual features and feature combinations. Two feature types, viz.: planar and ruled, and two feature interactions, viz.: combinations of planar features and combinations of ruled features are studied in detail, with parameters and algorithms to generate response surfaces presented. Validation studies on the generated response surfaces show average deviations less than 0.3 mm. The predicted response surfaces are then used to generate compensated tool paths by systematically translating the individual vertices in a triangulated surface model of the part available in STL file format orthogonal to the surface of the CAD model, and using the translated model to generate the optimized tool paths. These tool paths bring down the accuracy for most test cases to less than 0.4 mm of average absolute deviations. By further combining the MARS compensated surfaces with a rib offset strategy, the accuracy of planar features is improved significantly with average absolute deviations less than 0.25 mm.

Keywords: incremental forming; features; MARS; accuracy; SPIF; Tool path compensation

1. Introduction

Single Point Incremental Forming (SPIF) is a sheet metal prototyping process that can produce a wide array of sheet metal parts without the need for expensive dies and tools [1]. The process is based on the concept of incrementally deforming a sheet metal blank into a desired shape with the help of a CNC tool, usually a stylus with a hemispherical end, that follows a specified tool path. The generation of the tool path is of particular interest as it is directly related to the dimensional accuracy of the manufactured part and also defines other attributes, such as surface finish, forming limits, processing time and thickness variation [2, 3]. In particular, Rauch et al. have proposed an intelligent CAM tool path optimization method where process data are evaluated by CNC controllers to modify the basic CAM tool path in real time [2]. Skjoedt et al. proposed the use of helical tool paths for eliminating scarring caused by step downs in a z-level contouring tool path [4].

One of the key issues in incremental forming is that of the achievable accuracy. Jeswiet et al. report that, while most industrial parts require an accuracy of ± 0.5 mm, it is observed that parts produced by SPIF have significantly higher dimensional inaccuracies [1]. Several strategies to overcome shape and dimensional errors in incremental forming have been summarized by Micari et al., including the use of flexible support, use of counter pressure, multipoint and backdrawing incremental forming and use of optimized trajectories [5]. Bambach et al. proposed a combination of multi-stage forming and stress-relief annealing to improve the accuracy of a car fender section [6]. The accuracy of parts with areas containing positive curvature or planar faces can be improved

* Corresponding author. Tel.: +32 4 89 16 79 18. Fax: +32 16 32 29 86
E-mail addresses: amarkumar.behera@cib.kuleuven.be (A. K. Behera), johan.verbert@gmail.com (J. Verbert), bert.lauwers@mech.kuleuven.be (B. Lauwers), joost.duflou@mech.kuleuven.be (J. R. Duflou)

by reprocessing the workpiece [7] or using a reverse finishing operation [8]. However, this leads to a significant increase in the production time, and also yields a poor surface finish. Another method that has been proposed involves using measurements of the part to iteratively correct the CAD model by translating it by a scaled measure of the deviations for each individual point [9]. The drawback of using such a strategy lies in its lack of suitability for parts that need to be manufactured only once or in small batches, and the application of such a strategy would require making test parts, measuring them and then applying the correction strategy, possibly in an iterative procedure. Likewise, although Rauch et al. propose an online tool path optimization technique [2], the scope of their work in terms of accuracy is limited to the depth of the manufactured part and the surface roughness.

To overcome the limitations of the above techniques for improving the accuracy of parts produced by SPIF, Verbert et al. proposed the FSPIF (Feature Assisted Single Point Incremental Forming) method [7]. This method is based on the premise that different part features behave differently during incremental forming. A first level classification of features consists of planes, ribs, ruled and freeform features [7]. A more extensive taxonomy, taking into account geometric, orientation, location and process parameters, is provided by Behera at al. [10]. The FSPIF method generates an optimal single pass tool path for each feature in a part taking into account knowledge of the behavior of each feature.

The generation of an optimal tool path depends on the ability to predict the errors using an uncompensated tool path for the original CAD model of the part. Micari et al. have tried to model the errors at the bottom corner (illustrated in the SPIF process schematic in Fig. 1) and under forming of the bottom using geometrical parameters such as sheet thickness, part geometry and process variables such as tool diameter and step down [11]. However, in order to compensate tool paths for the entire part, it is necessary to have a mathematical tool in place that can predict deviations at individual vertices of the CAD model of the part. Several studies in incremental forming have involved the use of finite element analysis to predict the final shape and dimensional deviations [12, 13, 14]. Hadoush et al. have mentioned computation times for such analyses to vary from 16 hours to a few days for a simple pyramidal part of depth 20 mm with 40 incremental steps of 0.5 mm each, using implicit iterative algorithms [14]. The computation time for convergence is also dependent on the geometry and size of the part, and is a major limitation to the application of finite elements as a quick prediction tool.

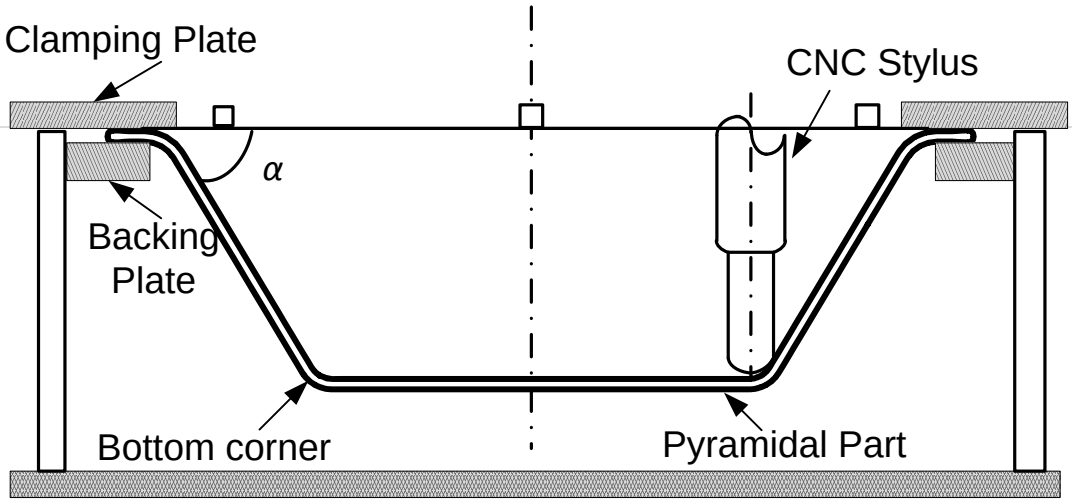

Fig.1. Schematic of single point incremental forming setup

In this paper, the authors propose the use of Multivariate Adaptive Regression Splines (MARS) as a fast and robust prediction tool. The use of MARS as a regression tool makes it possible to analyze accuracy data from measured parts available as a large dataset (~ (100, 000 - 500,000) points x (5-10) parameters), and automatically select the right variables for modeling the dimensional

deviations at individual vertices of the triangulated surface (STL) model of the part [15]. The models evolve as an expansion in product basis spline functions, which are automatically selected from the nature of variations within the dataset.

Response surfaces are predicted for individual features and feature combinations based on data collected from training sets. Compensated tool paths are then generated from the predicted response surfaces by systematically translating the individual vertices in the STL model of the part orthogonal to the STL model as suggested by Hirt et al. [9], and using the translated STL model to generate the optimized tool paths. Next, we present a set of tests performed on parts different from the training sets which show systematic improvement in accuracy behavior of features and their combinations.

All tests reported in this work are performed using standard, unidirectional contouring z-level tool paths, as shown in Fig. 2. A uniform increment in depth is provided at the end of each contour of the tool path, which is termed as a 'step down'. Besides, results are presented for a single material with a specified thickness. The proposed accuracy response surfaces can be calibrated for new materials and thicknesses with a limited set of new experiments following the procedure outlined in the paper for generating MARS response surfaces.

Further, the methodology outlined in this article can be used for carrying out accuracy compensation in complex 3D shapes as well. However, this requires an integrated approach such as the use of a graph topological framework, which can capture the effects of the presence of multiple features in a part and their interactions. Further, additional process steps such as tool path continuity aspects will need to be addressed for such shapes, which are beyond the scope of the present work.

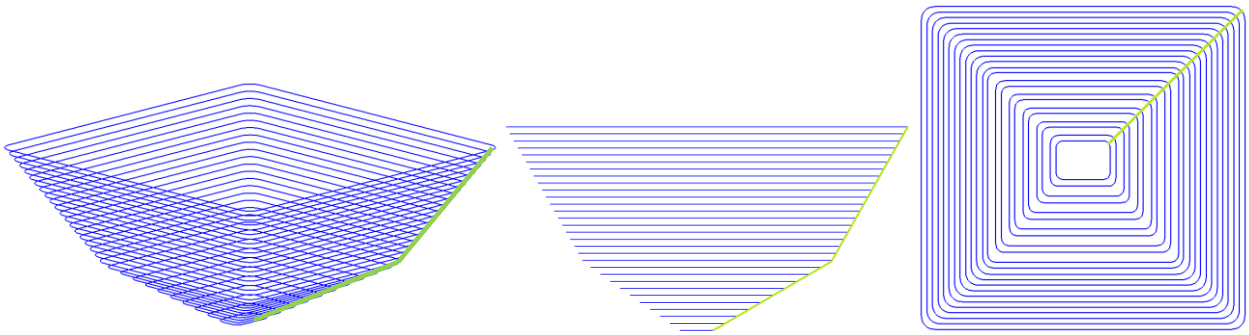

Fig.2. Contouring tool path for incremental forming of a two angled pyramid (from left to right: isometric, side and top views); starting points for each contour and the step down are marked with a green line

2. Relevance of features in incremental forming

A distinct set of features which exhibit a certain behavior during the forming process can be identified for parts formed by single point incremental forming. At the first level of the taxonomy developed for incrementally formed parts, part features may be classified as planes, ruled surfaces, freeform surfaces and ribs by considering the principal curvatures [16]. A more detailed classification takes into account orientation, location, curvature and process related parameters, which also affect the behavior of a feature [10]. A CAD package built in house on the Visual C # programming platform and discussed below in Section 2.1 is used to first detect features. The detected features can then be transformed to generate a compensated STL file which is used for generating the optimized tool paths.

2.1 Feature detection

The detection of features on a part is dependent on the CAD file format. While certain representations, such as those for analytic surfaces support the availability of feature related information, others such as surface meshes defined in a triangulated stereolithography (STL) or stereolithography contour (SLC) format, do not carry feature information. In analytic surfaces, a feature is composed of feature points, and as a matter of definition, normal directions are discontinuous at the surface boundary [17]. The feature points at the surface boundary can be connected to form a feature curve [17]. However, in a surface mesh, a collection of 0-dimensional cells (vertices), 1-dimensional cells (edges) and 2-dimensional cells (facets) in $\Re^3$ is used to create the surface definition. Of all the file formats for surface mesh representation, the STL format is one of the most commonly used [18]. It is a tessellated model of the outer surface of an object defined with the help of triangular facets. The work presented here is based on the STL file format. As the STL file format does not have provisions for storing feature types and feature IDs, the feature specific information is typically lost in the process of conversion from an analytic surface representation. An algorithm is therefore, needed for detection, which is presented below.

The first step in the feature detection algorithm involves calculation of the principal curvatures and normal at each individual vertex in the STL model of the part. This is done by following the procedure outlined by Lefebvre et al. [16]. The curvature tensor at a vertex *v* can be calculated as:

$$\Lambda(v) = \frac{1}{|A|}\sum_{edges}\beta(e)\|e \cap A\|\frac{ee^T}{\|e\|^2} \tag{1}$$

where $|A|$ is the surface area of the spherical zone of influence of the tensor and $\beta(e)$ is the signed angle between the normal vectors of the STL facets connected by the edge *e*, as illustrated in Fig. 3. $\beta(e)$ is positive for a concave surface and negative for a convex surface. The weight for the contribution by each edge is given by the factor $e \cap A$. The normal at each vertex is estimated as the eigenvector of $\Lambda(v)$ evaluated by the eigenvalue of minimum magnitude. The other two eigenvalues, k_{min} and k_{max} provide estimates of the minimum and maximum principal curvatures at *v*.

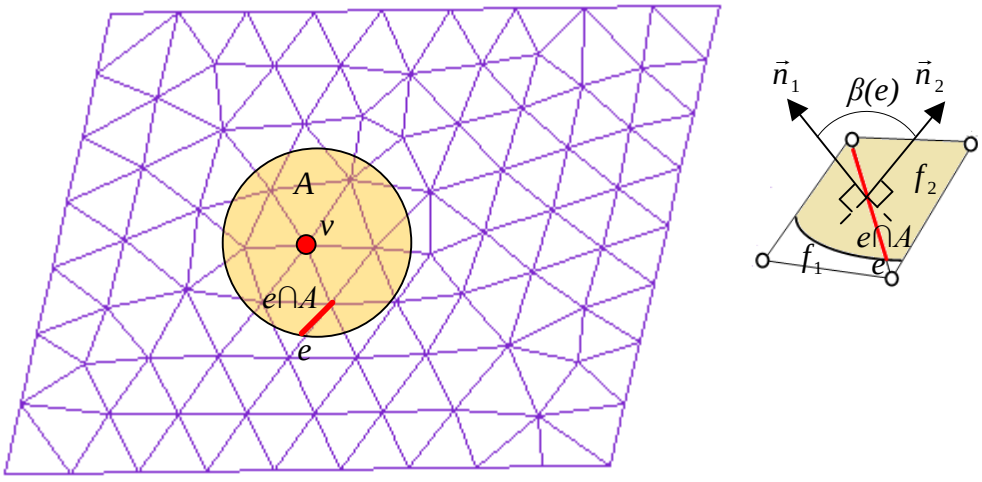

Fig.3. Estimation of curvature tensor using integration over a region *A*; the region $e \cap A$ is the part of the edge *e* common to the region A and is indicated by a bold red line; the figure on the right indicates the signed angle between the normal vectors, $\vec{n}_1$ and $\vec{n}_2$, of the STL facets f_1 and f_2, connected by the edge *e*

The second step in the feature detection algorithm is a segmentation and classification phase. A region growing algorithm with a combination of face based and edge based segmentation is used

following the procedure discussed by Varady et al. [19]. First, the edge based segmentation is used to find all vertices belonging to a rib. Vertices with the maximum principal curvature greater than a maximum threshold value ρ_{max}, or the minimum principal curvature lower than a minimum threshold value, ρ_{min}, are classified as rib vertices. Next, a face based algorithm is applied to the remaining vertices, where a feature object is created and allowed to accumulate vertices with similar curvature. The average curvature of the vertices in the feature object is then used to determine the classification of the feature object as a planar, ruled or freeform feature. A feature object with both principal curvatures equal to zero is classified as a plane, while a ruled feature is identified by having only one of the principal curvatures equal to zero. A freeform feature is identified as having non-zero principal curvatures, with the maximum principal curvature less than ρ_{max} and the minimum principal curvature greater than ρ_{min}.

The feature detection capabilities of the developed package enable the detection of 33 different types of features, as covered in the extensive taxonomy provided in [10]. This has enabled a framework for the mathematical compensation of these features and feature interactions.

2.2 Feature behavior

The behavior of different features during incremental forming is governed by their geometry, location on the workpiece, orientation, curvature and process parameters in use during incremental forming. To illustrate how the classified feature categories behave differently, a set of distinct feature behaviors, whose accuracy is later modeled in this work, is discussed below (the nomenclature used for the different features follows the taxonomy described by Behera et al. [10]):

Ordinary Non Horizontal Planar: An ordinary non horizontal planar feature is a planar feature that is oriented at an angle to the plane of the backing plate. The angle of the orientation is called the wall angle of the feature, denoted by ‘α’ in Fig. 1, and is below a critical wall angle for failure for the given material and sheet thickness. These planar faces show significant under forming as a result of bulging inwards caused by material spring back, as depicted in Fig. 4(a). The planar features are bounded by semi-vertical ribs on both sides and the deviations increase in magnitude towards the center of the feature and reduce to a minimum close to the ribs. This effect is also illustrated in Fig. 6.

Positive General Semi-vertical Ruled: A positive general semi-vertical ruled feature is a ruled surface with positive curvature. This feature is characterized by under forming induced due to the positive curvature and material spring back, as observed in Fig. 4(b). The magnitude of the deviations is different from ordinary non horizontal planar features for parts with the same dimensions.

Positive General Semi-vertical Ribs: Ribs are generally found at the intersection of two features. Positive general semi-vertical ribs are characterized by a positive curvature and observed to have high accuracy, typically less than 0.5 mm of under forming.

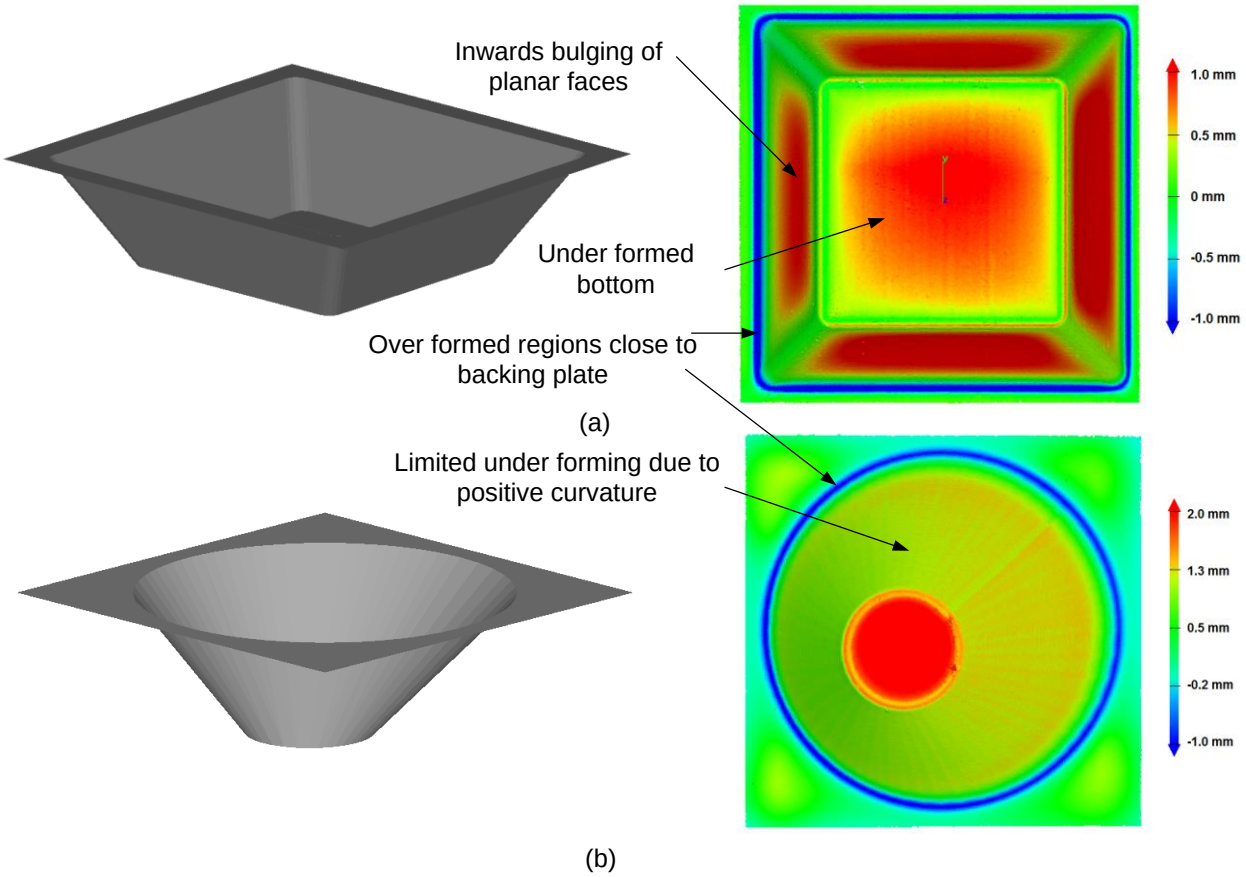

Fig.4. Accuracy behavior of different features during incremental forming: (a) Ordinary Non Horizontal Planar (b) Positive General Semi-vertical Ruled (*Isometric views of the part are shown on the left and color plots of accuracy are shown on the right*)

2.3 Interaction between features

Features in a sheet metal part are usually found together with neighboring features that can interact with them and thereby influence their final shape and accuracy. A set of selected interactions between features is discussed below (a matrix for these interactions showing feasible and infeasible interactions is described by Behera et al. [10]):

Combination of Ordinary Non Horizontal Planar features: A combination of two ordinary non horizontal planar features in the vertical direction (defined by the axis of the CNC stylus), with different wall angles and separated by an rib, is seen to produce the so-called ‘tent effect’, as shown in Fig. 5(a)). This results in the top planar feature being significantly under formed due to the inward pull generated by the lower planar feature in the case where the wall angle of the top planar face exceeds the lower planar feature. The top planar feature is over formed for the case where the top planar face wall angle is lower than the bottom face. Figure 5(a) shows an intermediate planar feature in green dotted lines just before the forming of the bottom planar feature. This intermediate planar feature has deviations only due to material spring back. On forming the bottom planar feature, the top planar feature is pulled further inwards. The intermediate horizontal rib is also seen to be displaced from its expected location, as is found at a lower depth.

Combination of Positive General Semi-vertical Ruled surfaces: Positive general semi-vertical ruled surfaces are more rigid than planar faces, and hence, the effect of the lower surface pulling the upper surface is less pronounced, as seen in Fig. 5(b). Besides, feature borders in the form of semi-vertical ribs may be absent for shapes such as combination of two quasi-identical cones or two closed ruled surfaces, which means that the inaccuracy at each sectional contour is a mere offset from the expected curve at the section.

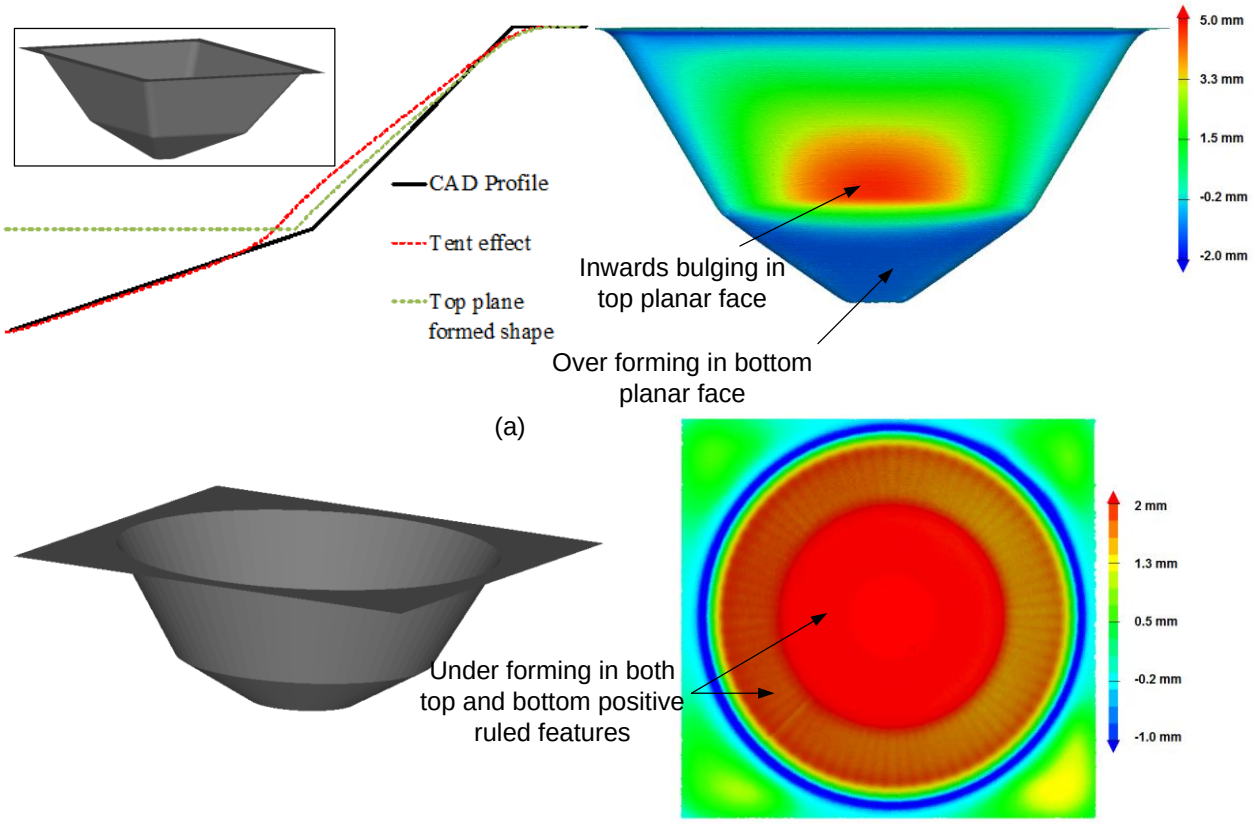

Fig.5. Accuracy behavior of feature interaction combinations (a) Combination of Ordinary Non horizontal Planar features (b) Combination of Positive General Semi-vertical Ruled surfaces (*Isometric views of the part are shown on the left and color plots of accuracy are shown on the right*)

3. MARS as a predictive tool for study of feature behavior and feature interactions

Generating optimized tool paths that reduce the errors due to geometry and material flow is facilitated by predicting the surface in an uncompensated single tool path pass procedure. Sectional views and close observation of the surface accuracy contour plots reveal the dependence on a significant number of parameters and parameter combinations that influence the final dimensional errors and shape of the part. Fig. 6 shows the sectional view of a pyramid taken at various depths depicting the nominal CAD model and the measured part in an uncompensated single pass tool path test. It can be seen that the errors, represented for individual points as $e_{x,y,z,}$ vary as a function of the depth, and also as a function of the distance from the semi-vertical ribs that define the boundaries of the four faces of the pyramid.

Likewise, it is seen that the wall angle has a significant influence on the accuracy profile. This is illustrated in Fig. 7(a) for four different planar faces with wall angles varying between 20° – 50° in a pyramid of depth 22.5 mm. It is seen that the accuracy is lower for higher wall angles, with increased under forming, while low wall angle features show areas of significant over forming. For a combination of non horizontal planar features, the difference in wall angle between the top planar face and bottom planar face, affects the accuracy, as shown in Fig. 7 (b) for planar faces with wall angle differences varying between 5° – 30° in a two angled pyramid of depth 67.5 mm. For other geometries, the curvature becomes an important parameter as well, as discussed in Sections 2.2 and 2.3.

3.1 Accuracy modeling using MARS

To model the accuracy for a given geometry or feature interaction combination with the most important parameters and their combinations, a statistical tool is required that enables flexible regression analysis of large data sets. Leathwick et al. have outlined the capabilities of Multivariate Adaptive Regression Splines or MARS for fitting complex, nonlinear relationships and in particular for incorporating interactions between variables [20]. The use of MARS also provides two immediate advantages that are relevant to the process, viz.:

i) MARS is a non-parametric regression technique, and hence does not assume a relationship between the predictor variables and response variable a priori. Rather it sifts through the data set and finds out the best possible relationship.
ii) MARS produces a continuous response surface with continuous first order derivative which is essential for predicting the final shape of a sheet metal surface.

MARS models take the form:

$$\hat{f}(x) = \sum_{n=1}^{N} c_n B_n(x) \tag{2}$$

The response variable is a weighted sum of basis functions $B_n(x)$, and the coefficients c_n are constants. The basis function $B_n(x)$ evolves as one of three possible forms: i) a constant, ii) a hinge function of the type max(0,x − k) or max(0,k − x), where k is a constant and max(p, q) gives the maximum of the two real numbers p and q or iii) a product of two or more hinge functions that models interactions between two or more variables. The hinge functions thus have knots given by the constants which are determined by a forward pass operation that initially over-fits the given data, and is followed by a backwards pruning step which identifies terms that are to be retained in the model. MARS models generated in this paper were fitted in R, a statistical software suite developed as a GNU project, with functions present in the ‘Earth’ library of R [21, 22].

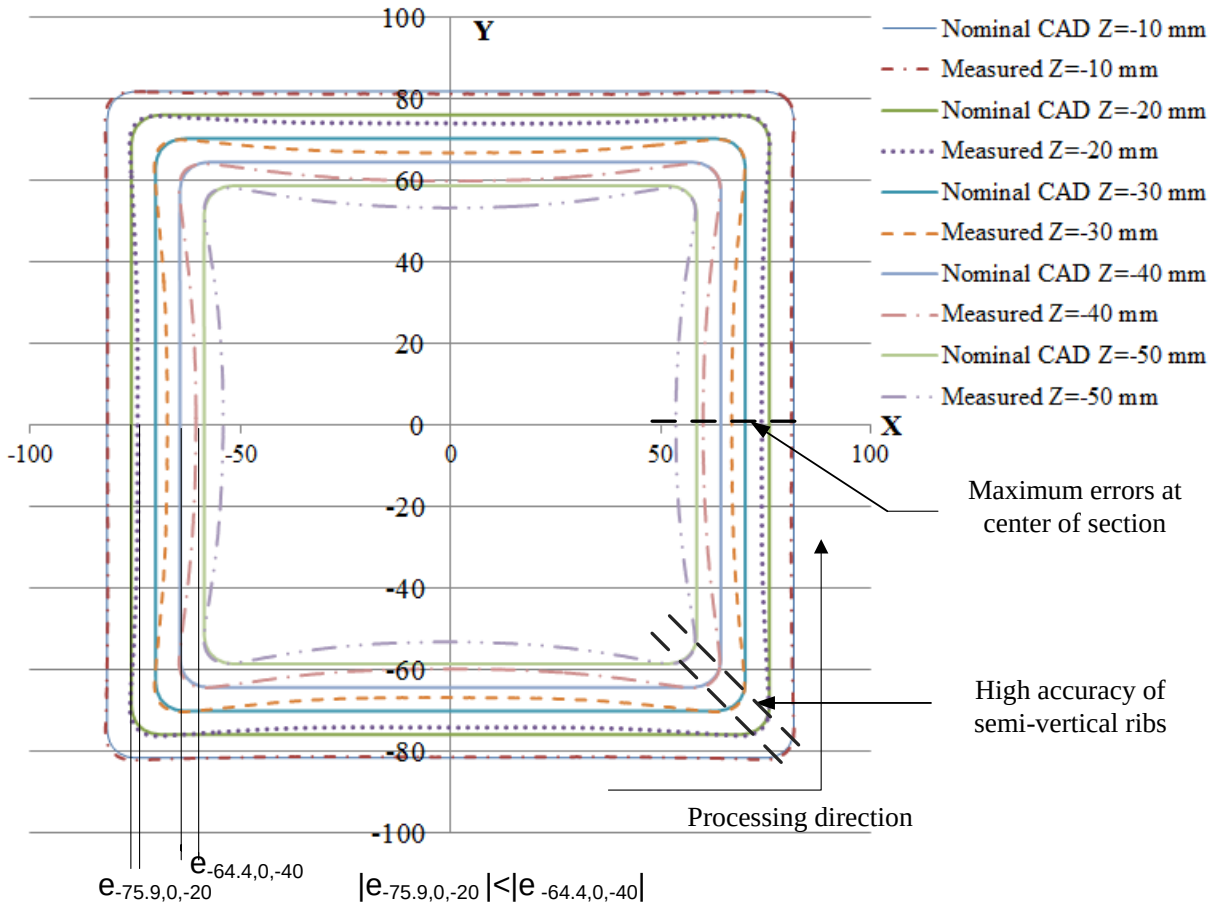

Fig.6. Dependence of accuracy in a pyramidal part with ordinary non horizontal planar faces made of AA 3103 of thickness 1.5 mm as a function of the depth and distance from the semi-vertical ribs ($e_{x,y,z}$ denotes the error at the nominal CAD model point (x, y, z) between the CAD model and the measured part made with an uncompensated tool path)

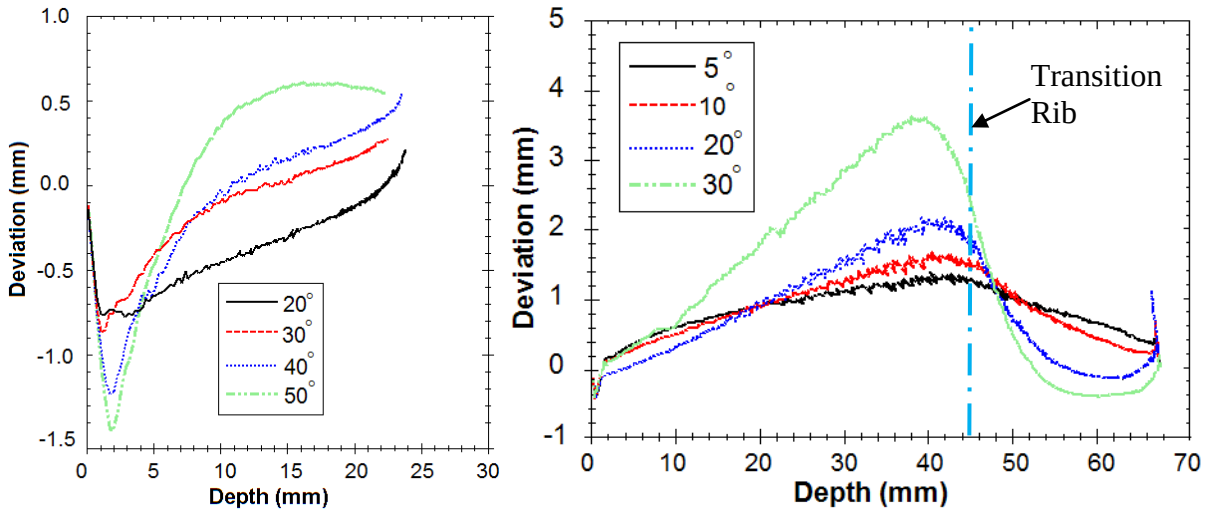

(a) (b)

Fig.7. Dependence of accuracy on (a) wall angle and nominal depth for a simple pyramid with non horizontal planar features and (b) wall angle difference for a two angled pyramid with combination of non horizontal planar features (location of transition rib shown as a dash-dot line), shown as a function of the depth of the part

3.2 Methodology of generation of MARS models

An integrated approach that combines experimental techniques with analysis on software tools that include a dedicated, customized CAD geometric modeler developed specifically for incremental forming applications, is used to generate the MARS models. The first step of the developed procedure involves identification of the parameters that are relevant to a given feature or feature combination. Once these parameters are identified, experimental tests with variation of the parameters are performed to manufacture parts on a 3-axis NC controlled milling machine. The obtained test results serve as training sets for the MARS models.

The manufactured parts are scanned with a laser scanner. The measurement accuracy of the scanner is specified as 15 µm. Focus Inspection v9.3, provided by Nikon Metrology NV, is used as the software platform for this purpose. The scanned point cloud serves as the measured model, which is then meshed in the software and compared to the nominal CAD model. This method for determining accuracy generates an accuracy file which contains details of the individual points in the nominal and measured point clouds, and deviations along x-, y-, and z- axes and the 3D deviation measured in a direction normal to the nominal model. The accuracy file, thus generated, can now be analyzed in the dedicated 'FSPIF' CAD platform developed specifically for incremental forming. FSPIF is an in-house software developed in Microsoft Visual C# 2008 Express Edition that enables several functionalities such as importing and manipulating STL files, point clouds and tool paths, detecting part features in STL files, generating relevant graphs such as thickness and accuracy variation within a part etc. Figure 8 shows a screenshot of the software depicting features detected on a two angled pyramidal part.

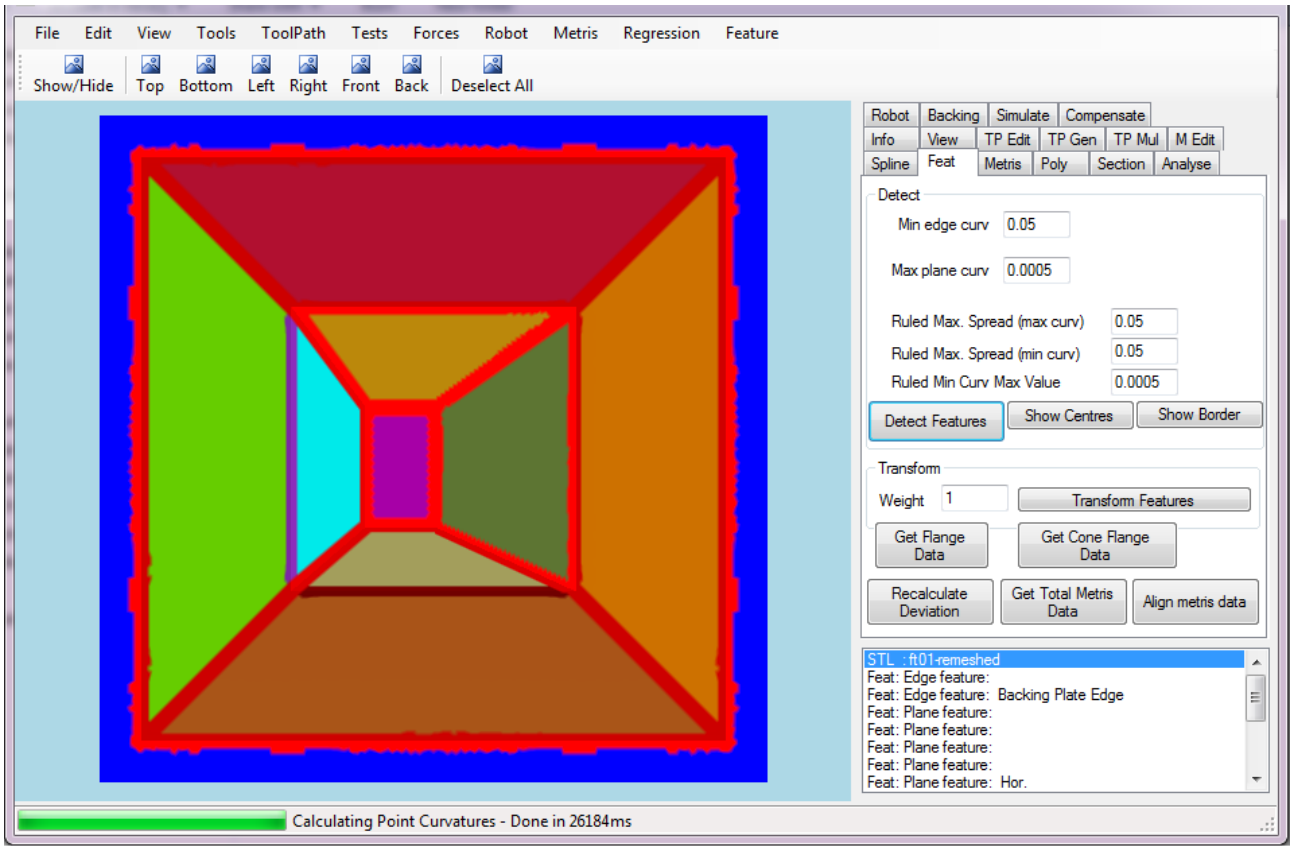

Fig.8. Feature detection in FSPIF CAD package interface for incremental forming

The accuracy file generated in Focus Inspection is imported within the FSPIF interface and linked to the STL model of the part. The linking is done for each vertex in the nominal model and a vertex

on the measured CAD model closest to the nominal vertex is found using KDTrees, which are multidimensional binary search trees for carrying out quick spatial comparisons using an associative searching technique [23, 24]. Features are detected on the STL model of the part, and each individual feature is now exported as an ASCII text file, and contains the accuracy data for the nominal CAD model vertices within the feature, and the value of the various parameters for each individual vertex, such as the wall angle, distance from the borders etc. These text files, containing the feature based accuracy data, are then analyzed within the GNU program, R, to generate the required MARS models. Figure 9 shows a schematic of the process for generating the training sets containing accuracy data for building the MARS models, while Figure 10 illustrates the subsequent steps for generating the MARS models and then using them to carry out accuracy improvement studies for specific test cases. The training sets generated in Fig. 9 create a generic MARS model for the specific feature, which can then be used for parts with new part designs containing the same feature type.

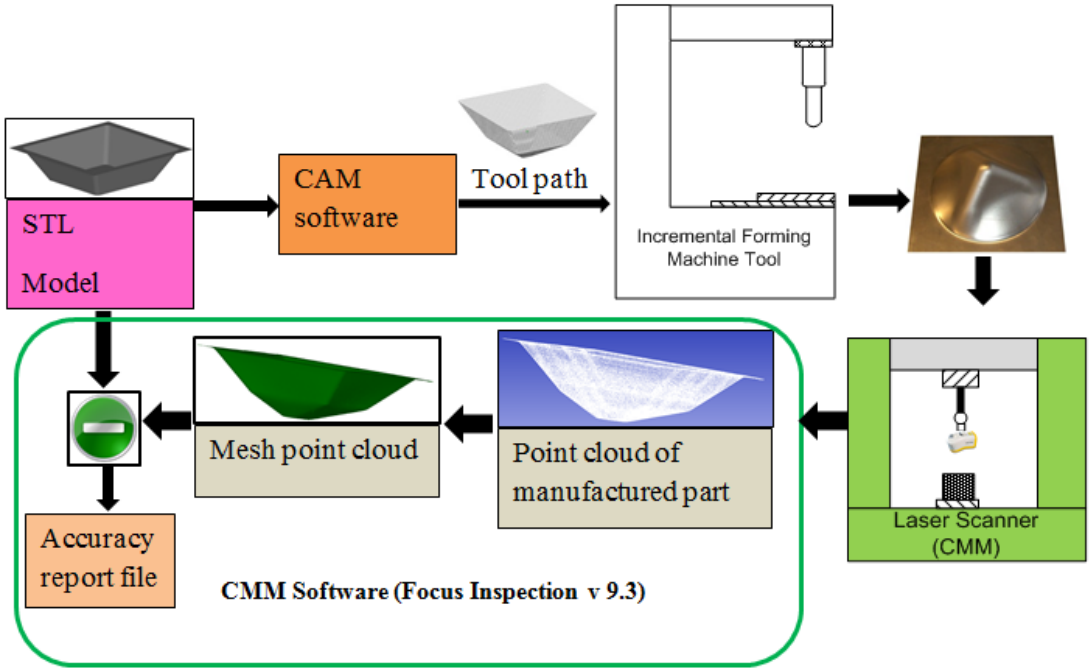

Fig.9. Methodology for generation of training sets containing accuracy data for building MARS models

3.3 MARS model for ordinary non horizontal planar features

The initial set of parameters influencing the accuracy of planar features at each vertex based on observations from experiments are: normalized distance from the point to the edge of the feature in the tool movement direction (d_b = D/(C+D) in Fig. 11), normalized distance from the point to the bottom of the feature (d_o = B/(A+B) in Fig. 11), total vertical length of the feature at the vertex (d_v = (A + B) in Fig. 11), total horizontal length of the feature at the vertex (d_h = (C + D) in Fig. 11), wall angle at the vertex (in radians), α and angle of the tool movement with respect to the rolling direction of the sheet (in radians), ω.

The determination of the distances to the feature borders in the horizontal and vertical directions requires the detection of the feature borders in the form of ribs, and intersecting the normal to the plane at the given STL vertex with the feature border. A set of three uncompensated tests was performed to train the MARS model. Two truncated pyramids with four faces as shown in Fig. 12 (a,b) with wall angles 60° and 65° respectively, and a part with planar faces as shown in Fig. 12 (c), were manufactured in AA 3103 sheet material with nominal thickness of 1.5 mm. A hemispherical

tool of radius 5 mm was used for all the tests along with a feedrate of 2 m/min, a tool rotation speed set to approximate rolling contact [1]. An oil based lubricant was applied during the process.

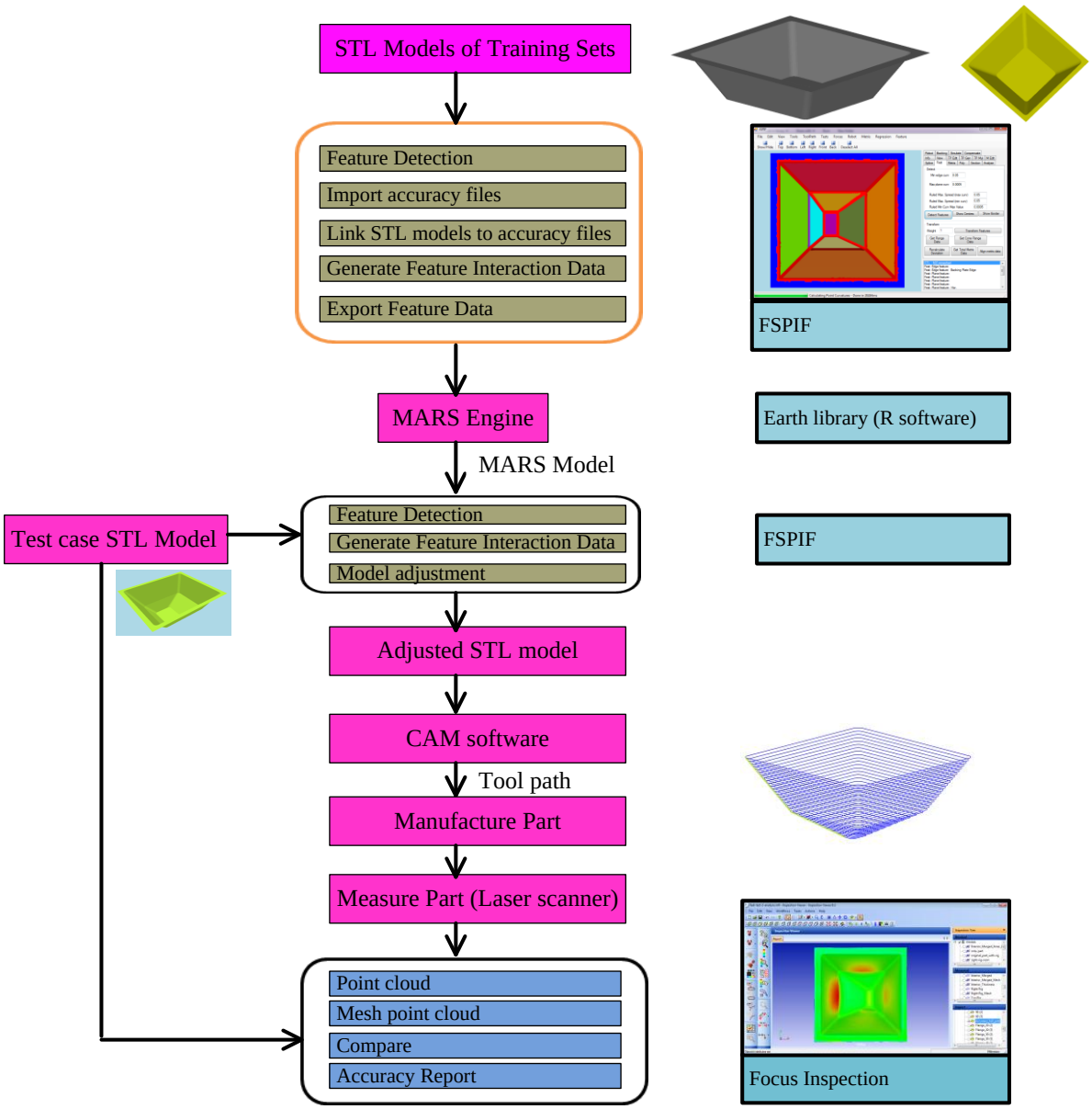

Fig.10. Flowchart illustrating the procedure for generation of MARS models and use of these models to improve accuracy of parts

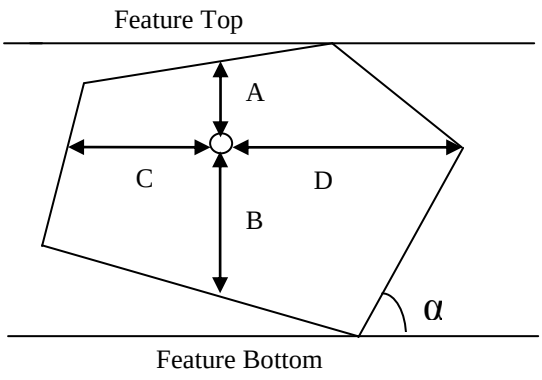

Fig.11. Geometrical input parameters for the MARS model of a non horizontal planar feature

The MARS model was trained with accuracy values of faces 1-4 of Fig. 12 (a) and Fig. 12 (c) and face 4 of Fig. 12 (b) yielding the following equation.

$$e = 2.4 - 0.76 * \max(0, d_b - 0.4) - 1.2 * \max(0, 0.4 - d_b) - 2.3 * \max(0, d_b - 0.78) + 2.8 * \max(0, d_b - 0.44) - 3.4 * \max(0, 0.44 - d_o) - 3.3 * \max(0, d_o - 0.65) - 0.058 * \max(0, d_h - 113) - 0.0082 * \max(0, d_h - 127) + 0.034 * \max(0, d_h - 143) + 0.055 * \max(0, d_v - 71) + 0.010 * \max(0, 71 - d_v) - 3.5 * \max(0, 1.1 - \alpha) \quad (3)$$

where, e = deviation at STL vertex

The model is independent of the angle of the tool movement with respect to the rolling direction of the sheet, which indicates that the sheet anisotropy did not significantly affect the accuracy of the planar features in the training sets used.

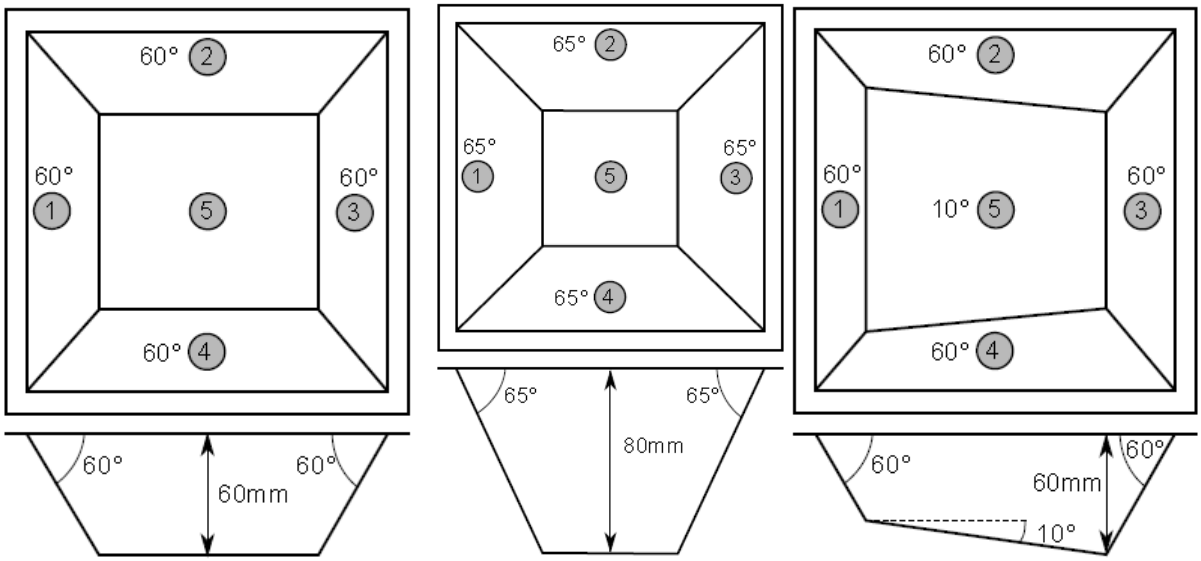

(a) (b) (c)

Fig.12. Training sets for generating the MARS model of a non horizontal planar feature

3.4 MARS model for positive general semi-vertical ruled features

Positive general semi-vertical ruled features, that are not in interaction with other features, can form closed surfaces without semi-vertical ribs as bounding features (e.g. a conical part) and hence, here, the input parameters for the model do not include the normalized distance from the STL vertex to the rib of the feature in the tool movement direction and the total horizontal distance. The model was trained with a ruled feature that was constructed by generating a ruled surface with the top circle having a center located at (0,0) and a bottom circle at a depth of 60 mm from the top circle with center located at (-10,-20), thereby varying the curvature and wall angle with upper and lower limits at 36° and 60°, as shown in Fig. 13.

The MARS model obtained by using the above training set is given below.

$$e = 1.2 - 1.9 * \max(0, d_o - 0.13) + 1.5 * \max(0, d_o - 0.26) + 0.0024 * \max(0, d_v - 13) - 0.054 * \max(0, 13 - d_v) - 0.0021 * \max(0, d_v - 30) + 0.0042 * \max(0, d_v - 78) - 5.6 * \max(0, k_m - (-0.012)) - 6.9 * \max(0, -0.012 - k_m) - 0.4 * \max(0, \alpha - 2.3) + 0.72 * \max(0, \alpha - 2.4) - 1.1 * \max(0, 2.4 - \alpha) - 1.6 * \max(0, \alpha - 2.4) + 3.1 * \max(0, \alpha - 2.5) \quad (4)$$

where, e = deviation at STL vertex, k_m = maximum principal curvature at the vertex, d_o = normalized distance from point to the bottom of the part, d_v = total vertical feature distance at the point, α = wall angle expressed in radians

The model is independent of the angle of the tool movement with respect to the rolling direction of the sheet, just as in the case of non horizontal planar features.

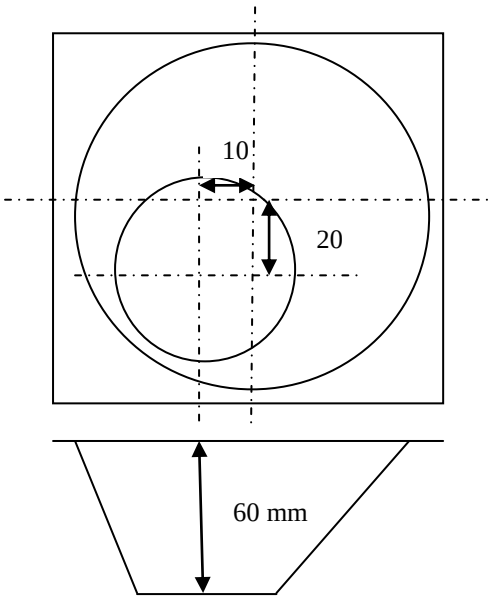

Fig.13. Training set for generating the MARS model of a positive general semi-vertical ruled feature

3.5 MARS model for a combination of ordinary non horizontal planar features

For a combination of non horizontal planar features in the direction of the tool-axis, as illustrated in Section 2.3, experimental tests reveal that the difference in wall angles between the top and bottom planar features decides the magnitude of the errors caused by the tent effect that is observed in the feature combination. The combination of these features is referred to as a 'combined feature' henceforth. It is also seen that the location of the transition rib also affects the shape and magnitude of the accuracy. Besides, the inaccuracy at a STL vertex is also seen to be dependent on the total length of the combined feature below it.

Keeping these physical effects in mind, three new distance parameters (as compared with the model for non horizontal planar features) are introduced as a function of: i) vertical distance from the STL vertex to the top of the feature, A, ii) the vertical distance from the STL vertex to the bottom of the feature, B, iii) vertical distance of the STL vertex in the top planar feature to the bottom of the combined feature, E and iv) vertical distance of the STL vertex in the bottom planar feature to the top of the combined feature, F, as shown in Fig. 14. A fourth new parameter is expressed as a function of the wall angles of the features. These parameters are given as: i) normalized vertical combined feature distance below the vertex, d_f, given by E/(A+E) for the top planar feature and B/(B+F) for the bottom planar feature, ii) total vertical combined feature length at the vertex, d_t, given by (A+E) for the top feature and (B+F) for the bottom feature, iii) normalized distance to transition horizontal rib, d_e, given by B/(A+B) for the top planar feature and A/(A+B) for the bottom planar feature, iv) wall angle difference, $\Delta\alpha$, given by (α-β) where α is the wall angle of the top planar feature, β is the wall angle of the bottom planar feature and α is greater than β. Besides, two parameters are dropped from the model in Section 3.3, viz.: i) normalized distance from the point to the bottom of the feature, d_o, and ii) total vertical length of the feature at the vertex, d_v.

The new normalized parameters, d_f and d_e, are introduced so as to be continuous functions of the depth of the part, which ensures proper training of the model using the accuracy data, and follows the physical observation that the manufactured part is a continuous surface. While d_f varies from a value of 1 at the top of the combined feature to a value of 0 at the bottom rib, d_e varied from a value of 1 at the top of the combined feature to 0 at the transition rib, and increases to 1 at the bottom of

the combined feature. On the other hand, d_o would have yielded a value of 0 for a point in the top feature infinitesimally close to the transition rib and a value of 1 for a point in the bottom feature infinitesimally close to the transition rib, while the accuracy value to be mapped for both these points very close to each other should be approximately the same. Likewise, d_t is a continuous function, while d_v is discontinuous at the rib. To generate the above parameters for the feature combination, calculations need to be carried out as explained in Algorithm 1 (see Appendix).

The MARS model for the feature interaction combination was trained with accuracy results from a two-angled truncated pyramid, with four different wall angle combinations, as illustrated in Fig. 15. The model generated with the four training sets from this experiment is given as:

$$e = 1.2 - 0.018 * \max(0, d_b - 109) - 0.0028 * \max(0, 109 - d_b) + 3.1 * \max(0, \Delta\alpha - 0.35) + 0.15 * \max(0, 0.35 - \Delta\alpha) + 4.5 * \max(0, d_f - 0.28) - 7.8 * \max(0, d_f - 0.57) - 2.1 * \max(0, 0.57 - d_f) - 30 * \max(0, d_f - 0.93) + 0.018 * \max(0, d_t - 46) - 0.0068 * \max(0, 46 - d_t) - 2.6 * \max(0, d_e - 0.18) + 4 * \max(0, 0.18 - d_e) + 2.4 * \max(0, d_e - 0.51) + 7.3 * \max(0, d_e - 0.89) - 5.6 * \max(0, 0.87 - \alpha) \quad (5)$$

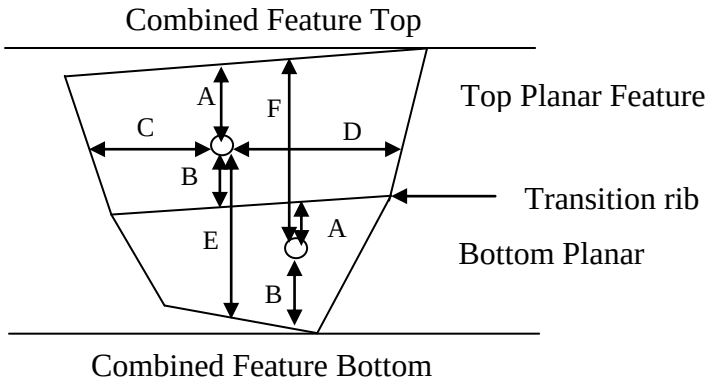

Fig.14. Geometrical input parameters for the MARS model of a combination of ordinary non horizontal planar features

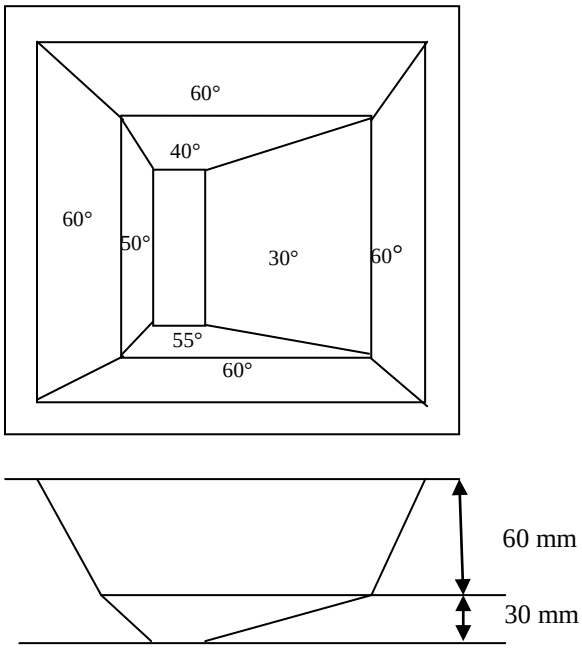

Fig.15. Training sets for generating the MARS model of a combination of ordinary non horizontal planar features

3.6 MARS model for a combination of positive general semi-vertical ruled features

The MARS model for a combination of positive general semi-vertical ruled features was trained with a set of six feature combinations formed by two angled cones with different top and bottom half wall angles and depths, as listed in Table 1. The set of parameters used for a combination of non horizontal planar features was also used here with only the horizontal distance parameters dropping out as explained in Section 3.4, viz.: normalized distance from the STL vertex to the edge of the feature in the tool movement direction and the total horizontal distance. The MARS model generated for the combination of ruled surfaces is given as:

$$e = 1.3 - 13 * \max(0, d_f - 0.94) + 0.4 * \max(0, 0.94 - d_f) - 0.04 * \max(0, d_t - 81) + 0.027 * \max(0, d_t - 134) - 0.041 * \max(0, 134 - d_t) + 7.8 * \max(0, \alpha - 2.2) - 18 * \max(0, \alpha - 2.6) - 12 * \max(0, \alpha - 2.7) + 3.4 * \max(0, 2.7 - \alpha) - 36 * \max(0, \Delta\alpha - 0.44) + 32 * \max(0, \Delta\alpha - 0.52) - 2.6 * \max(0, 0.52 - \Delta\alpha) + 4.1 * \max(0, \omega - 0.98) - 16 * \max(0, \omega - 1.1) + 3.3 * \max(0, 1.1 - \omega) \quad (6)$$

where, d_t = total vertical combined feature length at the point, d_f = normalized distance from point to bottom of combined feature, α = wall angle expressed in radians, $\Delta\alpha$ = wall angle difference between top and bottom ruled features expressed in radians, ω = angle with rolling direction expressed in radians

Table 1. Training sets for MARS model for combination of semi-vertical ruled features

Top Cone Wall Angle (°)	**Bottom Cone Wall Angle (°)**	**Top Cone Depth (mm)**	**Bottom Cone Depth (mm)**
20	10	15	7
35	20	30	12
45	40	50	20
50	25	50	20
60	30	50	20
65	55	50	20

4. Validation of MARS models

The MARS equations were used to predict formed surfaces made of AA 3103 of 1.5 mm thickness in uncompensated tests to verify their suitability for application to new parts. The prediction accuracies of the four models presented earlier are discussed in the sections below.

4.1 Ordinary non horizontal planar features

The MARS model for ordinary non horizontal planar features was used to predict the response surface for a pyramid with a wall angle of 55°. The predicted surface was compared to the measured surface from an uncompensated tool path test yielding an average positive deviation of 0.15 mm, and an average negative deviation of -0.25 mm. The average deviation was recorded as -0.13 mm, with outliers of 0.37 mm and -0.72 mm, and a standard deviation of 0.22 mm. Sectional views of the pyramid at Y= 0 are shown in Fig. 16.

4.2 Positive general semi-vertical ruled features

The response surface for a ruled surface part of depth 60 mm with continuously varying curvature and wall angle was predicted with Equation (4). The average positive deviation of the predicted surface with respect to the measured surface was observed to be 0.10 mm and the average negative deviation was seen at -0.07 mm. A mean deviation of 0.04 mm with outliers of -0.57 mm and 0.34

mm and a standard deviation of 0.10 mm were recorded. Sectional views of the part at Y= 0 are shown in Fig. 17. It may be noted that predictions are made only for the semi-vertical ruled feature. The rib close to the backing plate located between the depths z = 0 mm to z = -3 mm and the rib close to the horizontal bottom planar surface located between z = -57 mm to z = -60 mm are not predicted by the model as they are a different feature and detected as such within FSPIF.

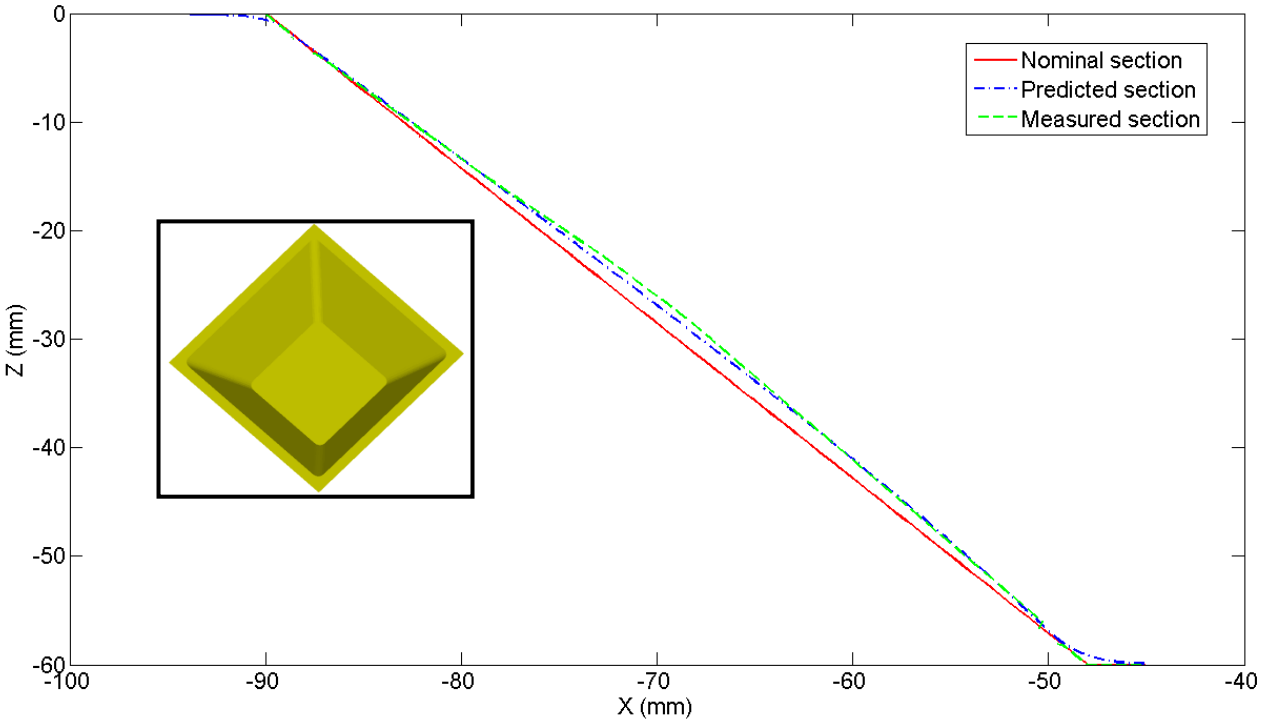

Fig.16. Sectional views of a pyramidal part taken at Y=0, showing nominal CAD, MARS predicted and measured part sections

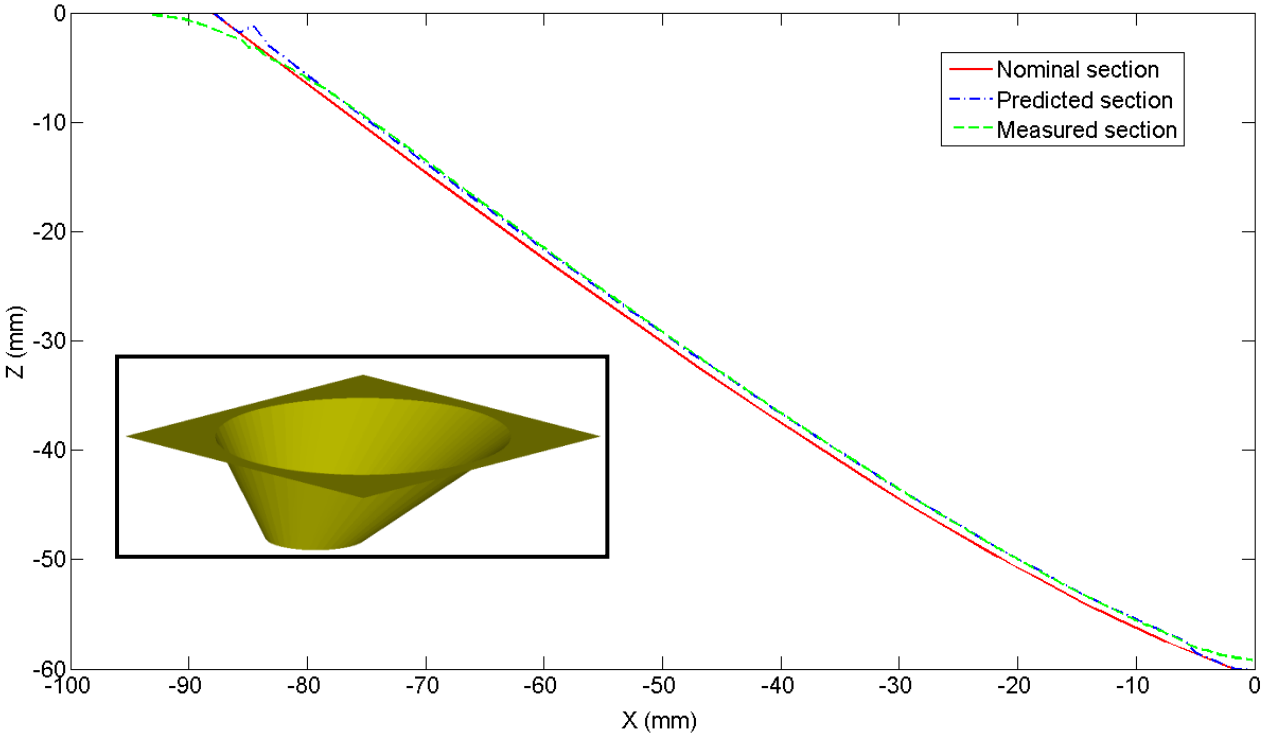

Fig.17. Sectional views of a generic ruled surface part taken at Y=0, showing nominal CAD, MARS predicted and measured part sections

4.3 Combination of ordinary non horizontal planar features

A planar face with a wall angle of 55° and depth 60 mm in combination with another planar face with a wall angle of 30° and depth 30 mm was used as to verify the model given in Equation (5). The average positive deviation observed was 0.25 mm and the average negative deviation was -0.37 mm, with a mean of -0.23 mm and a standard deviation of 0.34 mm. The maximum outliers were recorded as 0.65 mm and -0.99 mm. Sectional views of the two angled pyramid at Y= 0 are shown in Fig. 18.

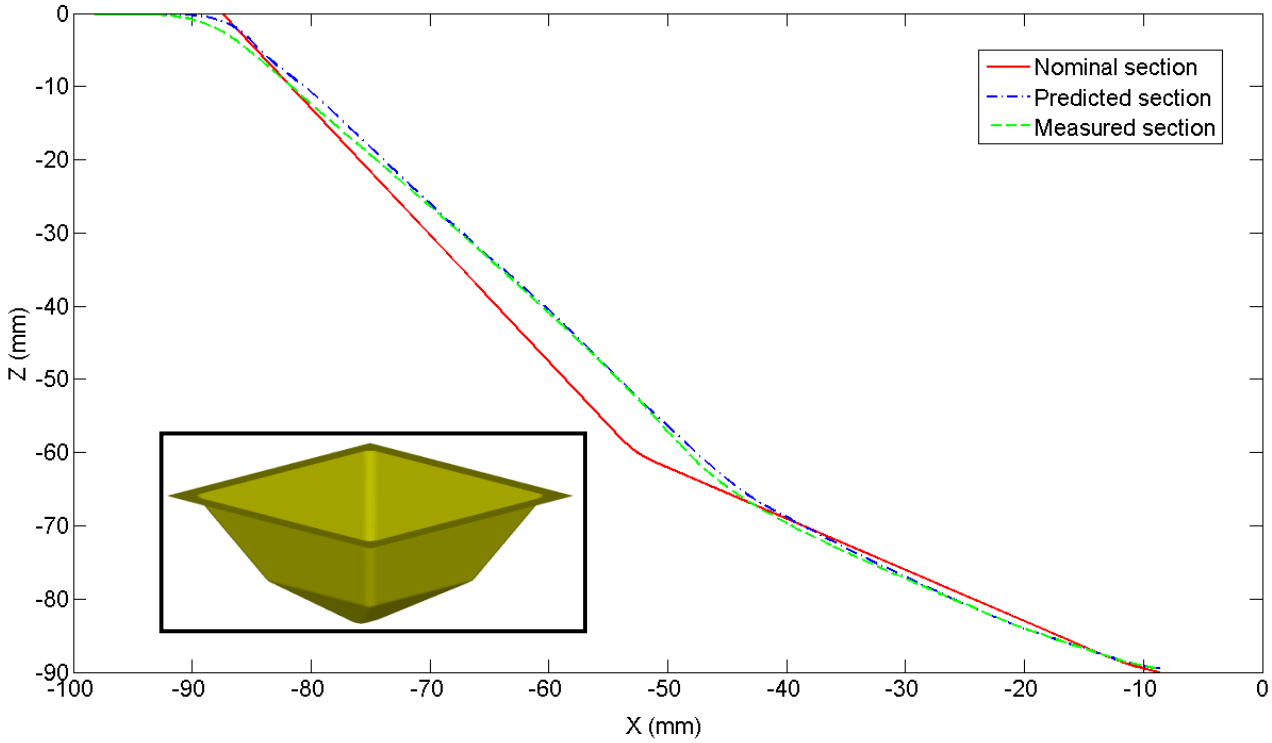

Fig.18. Sectional views of a two angled pyramidal part taken at Y=0, showing nominal CAD, MARS predicted and measured part sections

4.4 Combination of positive general semi-vertical ruled features

Predictions for a two angled cone with a top half wall angle of 55° and depth 50 mm and bottom half wall angle of 30° and depth 20 mm using Equation (6) showed an average positive deviation of 0.14 mm and an average negative deviation of -0.24 mm with a mean of 0.06 mm. Outliers were seen at -0.46 mm and 0.33 mm with a standard deviation of 0.18 mm. Sectional views of the two angled cone at Y= 0 are shown in Fig. 19.

5. Tool path compensation results

5.1 CAD Model adjustment and generation of compensated tool paths

The generation of compensated tool paths that increase the accuracy of parts manufactured by incremental forming can be achieved, in many cases, by adjustment of the CAD model of the part. This adjustment is done by taking individual vertices in the STL model of the part and translating them proportional to the deviation corresponding to that vertex as predicted by the MARS model. Consider a nominal point vector $\vec{n}$ and a corresponding predicted point by the MARS model $\vec{p}$ as illustrated in Fig. 20. The predicted point is generated in the direction of the normal to the feature.

Given that the deviation vector between the nominal and predicted points is denoted as $\vec{d}$, we can then generate a translated point in the opposite direction of the feature normal $\vec{t}$ (= $\vec{n}$ - k. $\vec{d}$) [9], using the deviation $\vec{d}$ scaled by a compensation factor 'k' which can be adjusted for individual features or feature combinations based on experimental knowledge. The adjusted model is now used to generate compensated tool paths.

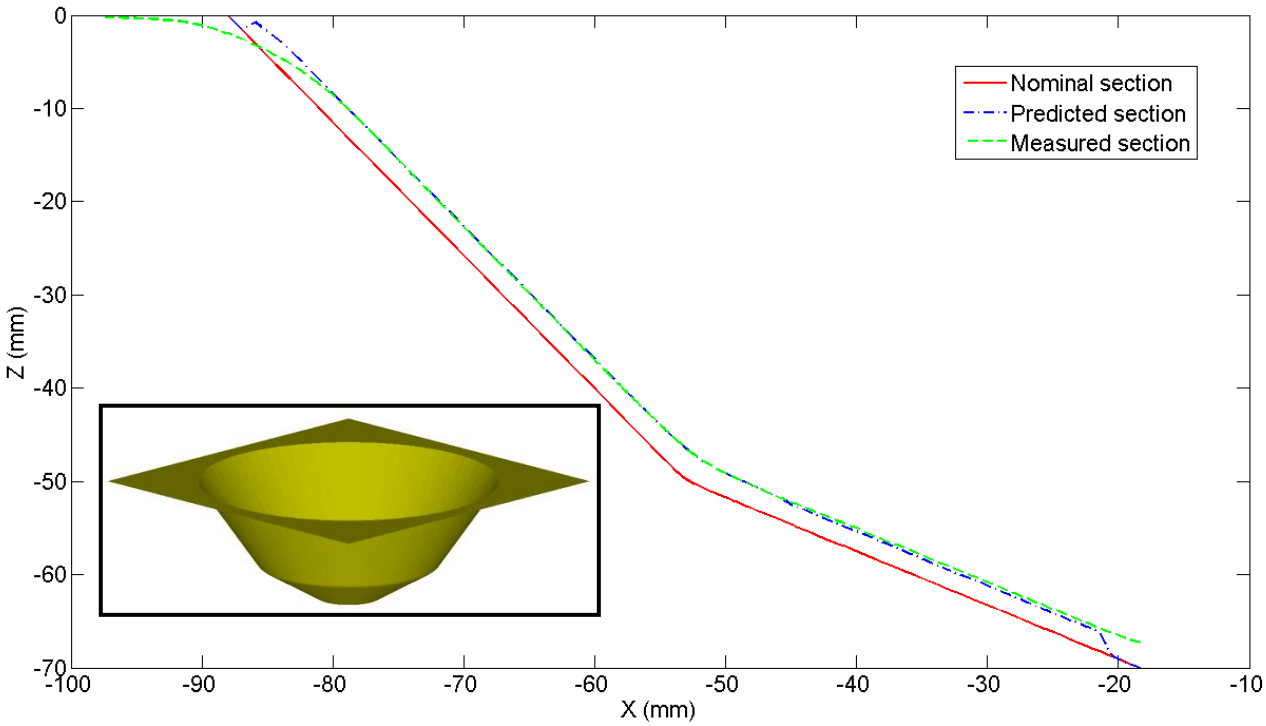

Fig.19. Sectional views of a two angled conical part taken at Y=0, showing nominal CAD, MARS predicted and measured part sections (part is shown in set)

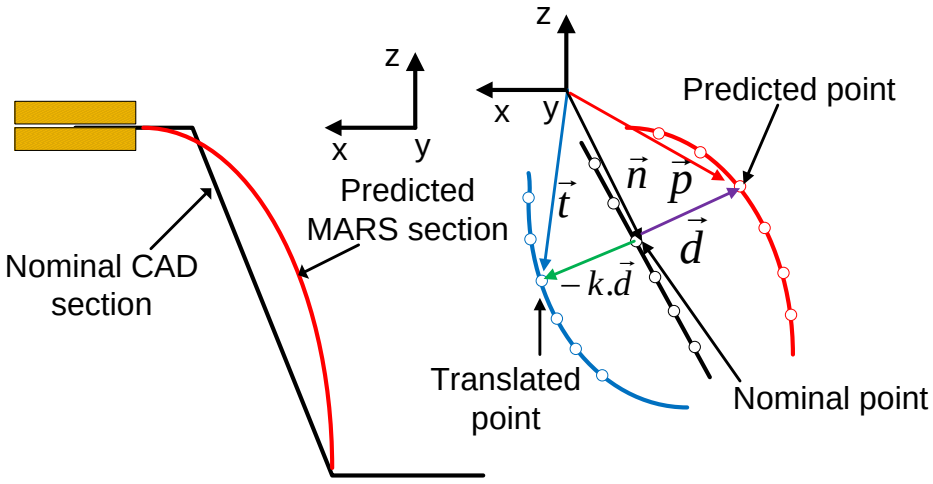

Fig.20. Translating vertices in STL model using MARS prediction and nominal CAD model

5.2 Results of application of compensated tool paths

Compensated tool paths were generated using Equations (3)-(6) for predicting the uncompensated response surface followed by model adjustment with appropriate compensation factors. All tests were performed on AA 3103 sheets of thickness 1.5 mm on a stiff three axis CNC milling machine

at a feed rate of 2 m/min and constant step down depth of 1 mm. Fig. 21 shows an example of tool path compensation for ordinary non horizontal planar features. Results for different features and feature interactions are discussed below.

5.2.1 Tool path compensation for ordinary non horizontal planar features

A pyramid of wall angle 55° was made using an uncompensated tool path and using the MARS prediction of Equation (3). Results shown in Fig. 22 indicate that the under forming of the planar faces is significantly reduced. Table 2 lists the deviations recorded in both tests.

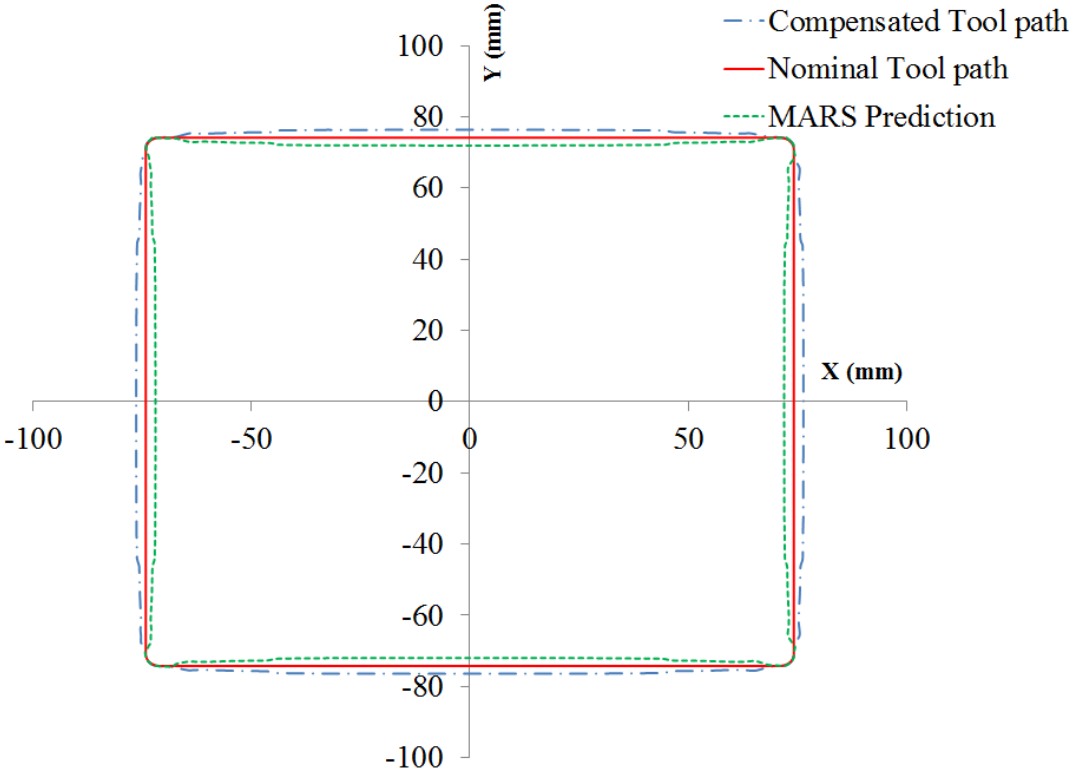

Fig.21. Generation of compensated tool path for ordinary non horizontal planar features (contours at depth Z= -18.6 mm are shown along with the MARS predicted section)

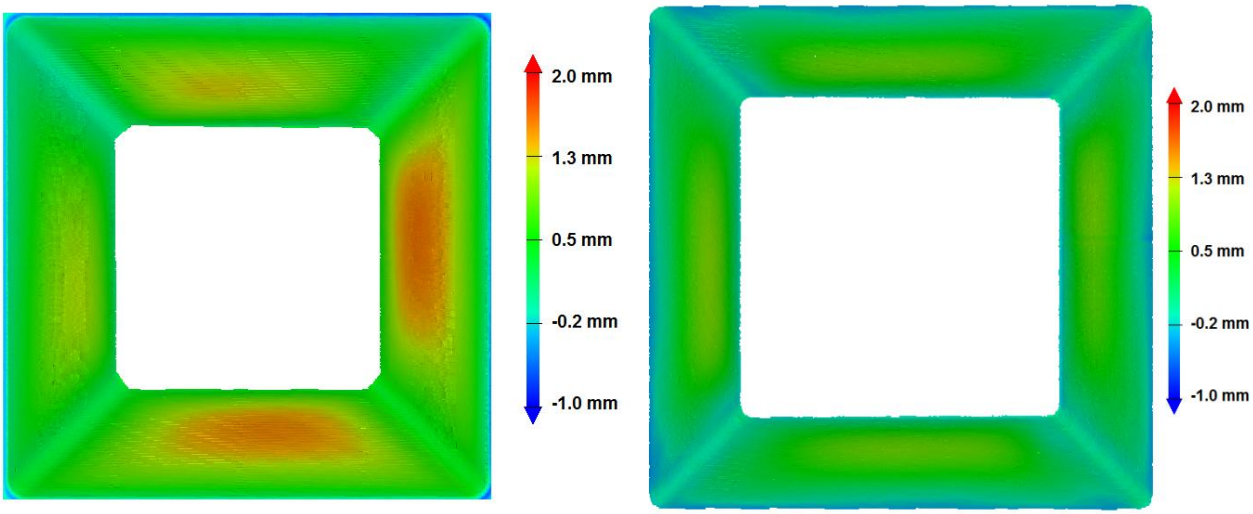

(a) (b)

Fig.22. Top view of accuracy color plots showing results of (a) uncompensated tool path test and (b) compensated tool path test using MARS predictions for ordinary non horizontal planar features

5.2.2 Tool path compensation for positive general semi-vertical ruled features

The MARS model in Equation (4) was used to manufacture a ruled surface similar to Fig.13 but with different offsets, viz. 15 mm and 25 mm for the lower circle, giving wall angles between 32° and 66°. A compensation factor ('k') of +1 was used. The tool paths at a specific depth are seen to be an offset from the nominal uncompensated cross-section, with the offset determined by the prediction for the deviation at each individual vertex, as illustrated in Fig. 23. The shape of the compensated tool path follows the shape of the cross-section at that depth. On applying the tool path, the maximum deviation found on the part was observed as 0.42 mm, thereby indicating that the under forming is significantly removed. Color plots illustrating this improvement are shown in Fig. 24.

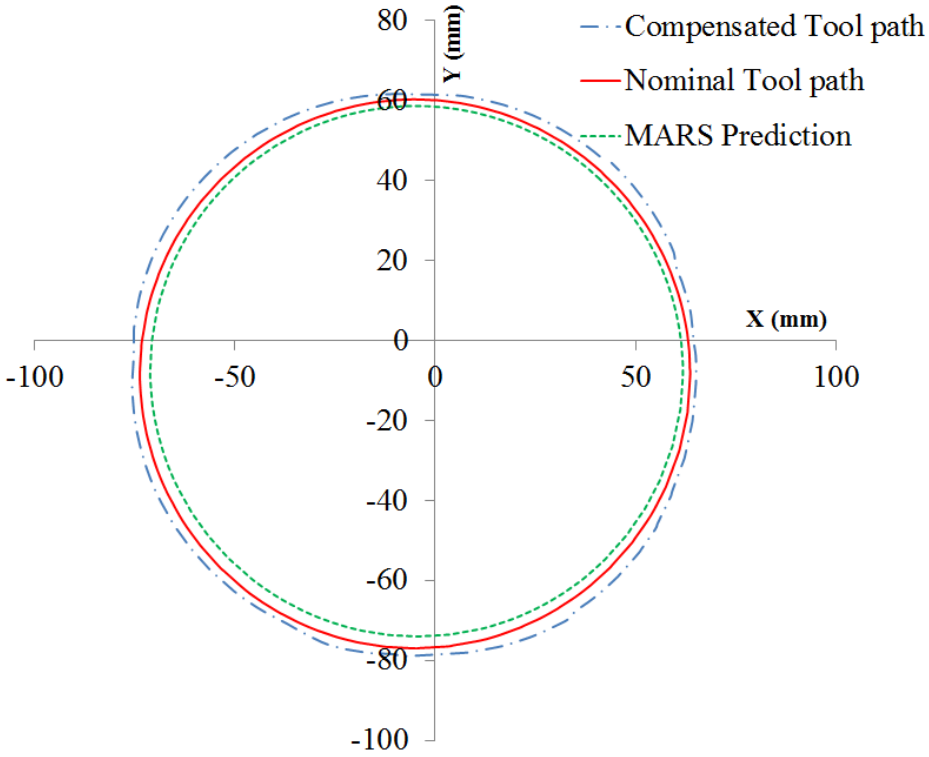

Fig.23. Generation of compensated tool path for positive general semi-vertical ruled features (contours at depth Z= -20 mm are shown along with the MARS predicted section)

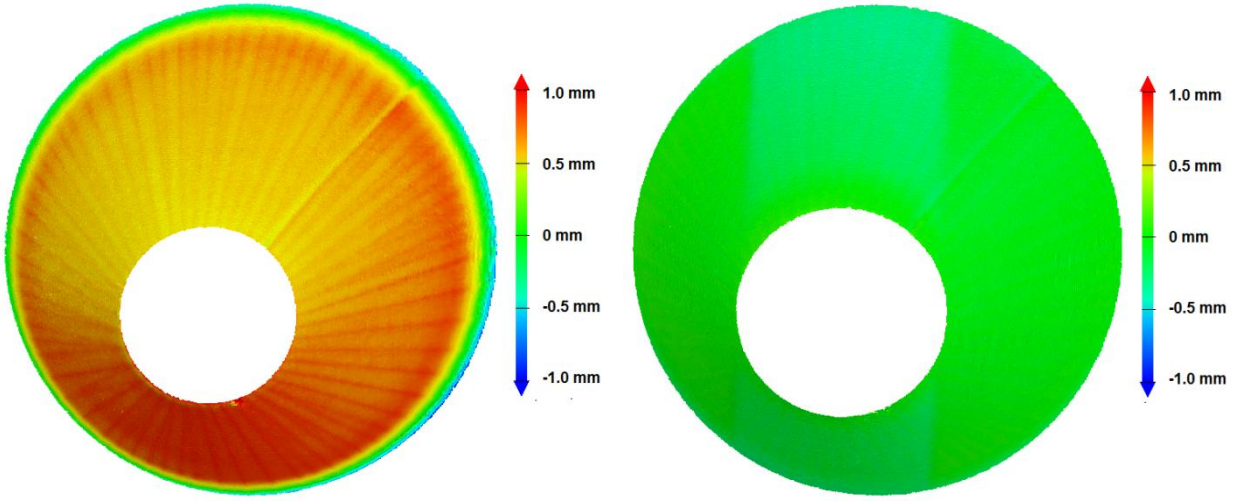

(a) (b)

Fig.24. Top view of accuracy color plots showing results of (a) uncompensated tool path test and (b) compensated tool path test using MARS predictions for positive general semi-vertical ruled features

5.2.3 Tool path compensation for a combination of ordinary non horizontal planar features

The MARS model in Equation (5) was used to manufacture a two angled pyramid with a top half wall angle of 55° and depth 45 mm and bottom half wall angle of 25° and depth 22.5 mm. A compensation factor of +1 was used. On applying the tool path, the average positive deviation shows an improvement of approximately 1 mm, thereby indicating that the under forming is mostly removed. Fig. 25 shows a color plot comparing the two test results.

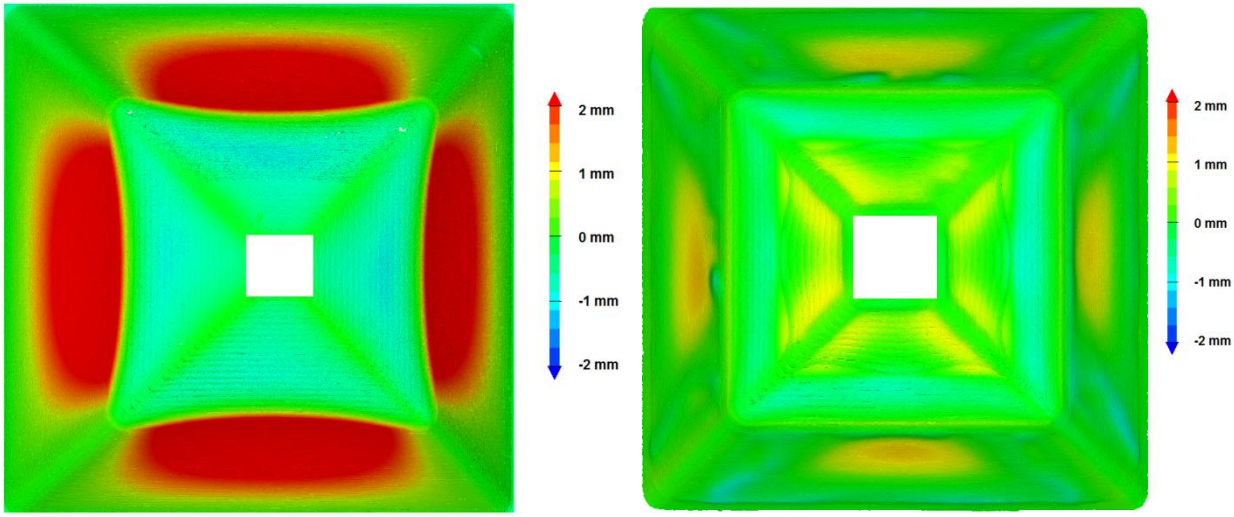

(a) (b)

Fig.25. Top view of accuracy color plots showing results of (a) uncompensated tool path test and (b) compensated tool path test using MARS predictions for a combination of ordinary non horizontal planar features

5.2.4 Tool path compensation for a combination of positive general semi-vertical ruled features

The MARS model in Equation (6) is used to manufacture a two angled cone with a top half wall angle of 55° and depth 50 mm and bottom half wall angle of 30° and depth 25 mm with a compensation factor of +1. While the uncompensated test shows significant under forming in both the top and bottom surfaces, the compensated test shows mild over forming in the top surface and fairly good geometrical accuracy in the bottom feature.

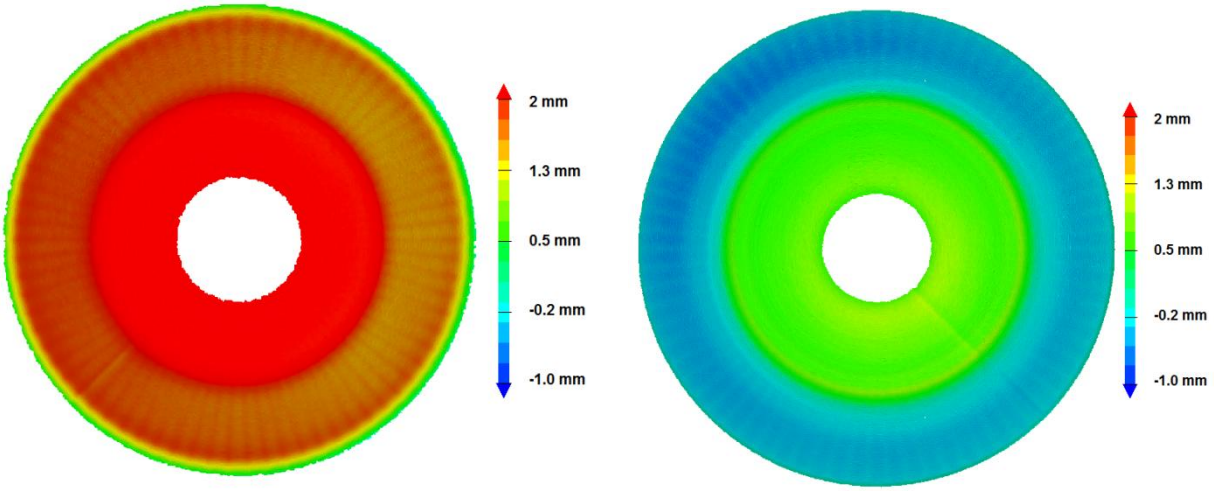

(a) (b)

Fig.26. Top view of accuracy color plots showing results of (a) uncompensated tool path test and (b) compensated tool path test using MARS predictions for a combination of positive general semi-vertical ruled features

5.2.5 Rib offset tool path compensation strategy

The accuracy plots of the pyramids show that inaccuracies can be observed in the regions close to the semi-vertical and horizontal ribs. The average deviation in these ribs was observed to be 0.2 mm. Hence, a strategy to improve the continuity of the tool paths near the ribs and to account for the inaccuracy of the ribs was devised. This involves offsetting the CAD model of the part first by a magnitude equal to the average deviations found in the ribs. The MARS compensation is then performed on this offset section as illustrated in Fig. 27. By using this strategy, the maximum deviations of the non horizontal planar features in both a simple pyramid and a two angled pyramid were brought down to less than 1 mm, as visible from the accuracy color plots in Fig. 28.

Table 2. Comparison of accuracies with different tool path strategies *(All dimensions are in mm)*

Part type	Features/ Feature interactions	Tool path strategy	Average Positive Deviation	Average Negative Deviation	Maximum Deviation	Minimum Deviation	Average Deviation	Standard Deviation
Simple Pyramid	ONHP	Uncompensated	0.748	-0.223	1.596	-0.843	0.632	0.507
Simple Pyramid	ONHP	MARS compensation (Equation 3)	0.440	-0.141	1.039	-0.466	0.242	0.364
Ruled surface	PGSVR	Uncompensated	0.673	-0.688	1.843	-1.563	0.533	0.457
Ruled surface	PGSVR	MARS compensation (Equation 4)	0.027	-0.115	0.429	-0.381	-0.081	0.100
Two angled pyramid	ONHP-ONHP	Uncompensated	1.377	-0.450	4.126	-1.349	0.764	1.268
Two angled pyramid	ONHP-ONHP	MARS compensation (Equation 5)	0.362	-0.222	1.099	-0.690	0.076	0.378
Two angled cone	PGSVR-PGSVR	Uncompensated	1.669	-0.389	2.379	-1.462	1.614	0.495
Two angled cone	PGSVR-PGSVR	MARS compensation (Equation 6)	0.349	-1.112	0.661	-1.512	-0.737	0.677
Simple Pyramid	ONHP	Offset MARS	0.248	-0.158	0.570	-0.535	0.160	0.222
Two angled pyramid	ONHP-ONHP	Offset MARS	0.218	-0.151	0.669	-0.790	0.042	0.230

ONHP – Ordinary Non Horizontal Planar
ONHP-ONHP – Combination of ordinary non horizontal planar features
PGSVR – Positive General Semi-Vertical Ruled
PGSVR-PGSVR – Combination of positive general semi-vertical ruled surfaces

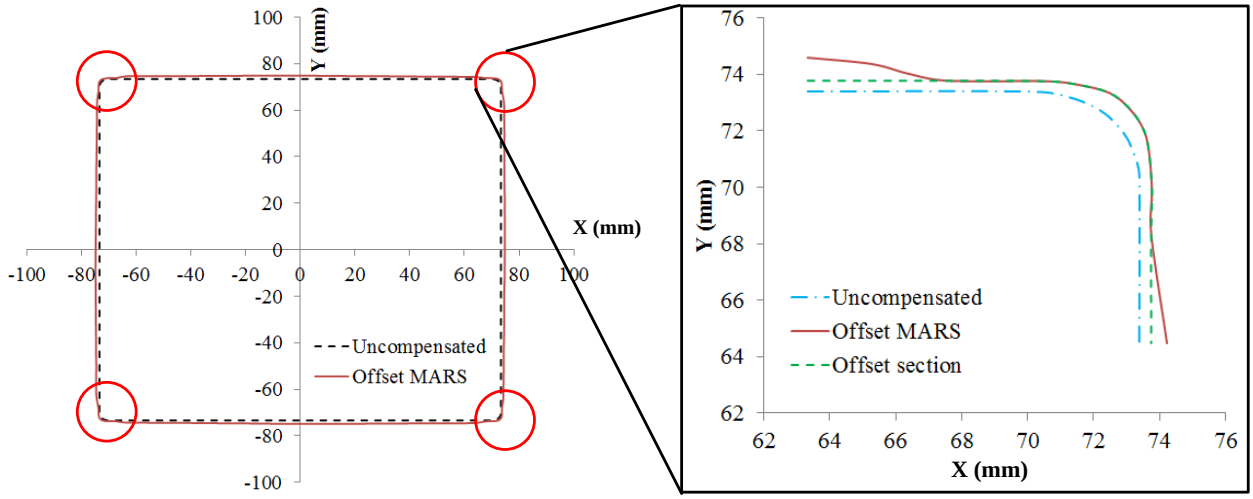

Fig.27. Applying the MARS method on an offset section to compensate for the inaccuracy of ribs; section shown is located at z=-20 mm on a planar face with wall angle of 45°

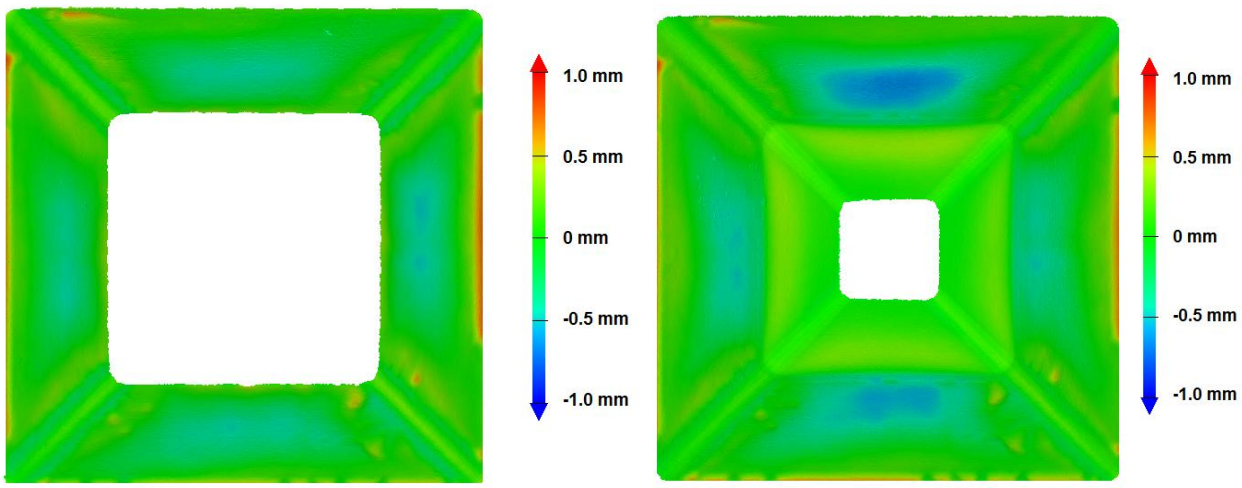

(a) (b)

Fig.28. Accuracy plots of (a) a simple pyramid of wall angle 55° and (b) a two angled pyramid with wall angles 55° and 45° using an offset MARS tool path as illustrated in Fig. 27

6. Limitations and Future scope

One of the basic issues in Single Point Incremental Forming is the process limits for part manufacture. For a given material and thickness, when using simple contouring tool paths, parts can be manufactured with a maximum achievable wall angle as discussed by Jeswiet et al. [1]. The process limits for part manufacture also limit the applicability of the MARS technique. For parts with wall angles slightly below the critical wall angle for failure, the compensation of the STL file for improving accuracy results in a compensated geometry that has a zone with wall angle greater than the critical wall angle for failure. This issue is illustrated in Fig. 29, where it is seen that the wall angle at a depth close to the top of the part, α^C, is larger than the wall angle of the nominal CAD section, α^N.

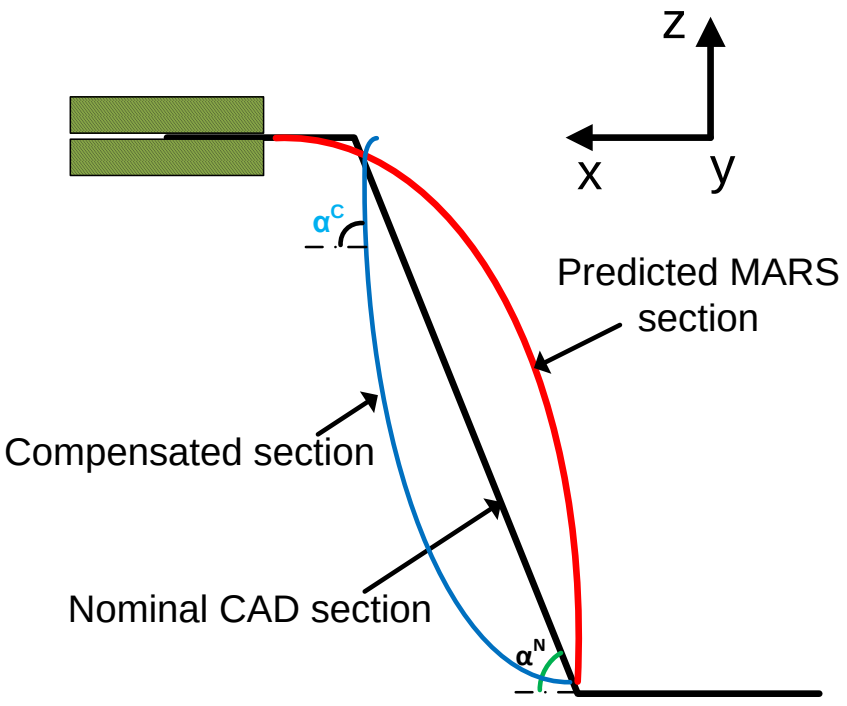

Fig.29. Compensated section showing wall angle higher than the wall angle of the nominal section

One of the solutions to this problem is to make the part in multiple steps as suggested by Duflou et. al [25]. However, in that case, the MARS model equations developed for single step tool paths will no longer be valid, and new training sets will have to be used that use the accuracy data from multi-step tool paths to predict the response surface. Nevertheless, the methodology used for doing so will still follow the guidelines outlined in this work.

Experiments also show that the accuracy of an incrementally formed part also depends on the material properties and thickness. In the current work, the response surface MARS methodology was illustrated for a specific material and thickness. As part of future research targets, the response surfaces can be calibrated to generate generic error correction functions, as functions of well-chosen material properties and sheet thickness.

7. Conclusions

This article presents the use of Multivariate Adaptive Regression Splines or MARS as a tool to predict the formed surface in single point incremental forming without actually forming the part. The prediction of the formed surface depends on the type of feature and interaction between features. The detection of features is the first step in the proposed method. A custom CAD package has been built that enables feature detection on the triangulated STL model of a part and implementation of the MARS method.

Models have been built to predict the formed surface for planar and positive curvature ruled features and combinations thereof. These models are dependent on several variables in the part geometry and process parameters. The evaluation of distance parameters in these models requires identification of feature borders, which typically are ribs. Further, the combination of features poses the additional problem of generation of distance parameters for the combined feature. This necessitates an algorithm which determines the correct points of intersection of the feature normal with the feature borders for the evaluation of the distance parameters.

It is possible to generate compensated single pass tool paths using MARS predictions by appropriate translation of the vertices in the STL model of the part. A compensation factor of +1 has proved useful for a number of case studies, and thus provides a good case for the application of this technique in a fast and robust manner with little user input. Besides, the compensated tool paths have helped bring down the average positive and negative deviations to less than 0.4 mm for several test cases. Further, the MARS tool paths can be combined with intelligent offsetting of the part features to further improve the accuracy.

One of the primary limitations of the MARS method lies in the manufacture of parts that are very close to failure, where the compensated surface may have zones with wall angles greater than the critical wall angle for failure. This limitation may be overcome by the use of multi-step tool paths in conjunction with the MARS technique. However, this requires additional research, and offers potential for further improving tool paths for incremental forming.

Acknowledgements

The authors gratefully acknowledge financial support from the Fonds Wetenschappelijk Onderzoek (FWO) – Vlaanderen, and the collaboration on this project with Prof. Hugo Sol, Jun Gu and Ioannis Vasilakos of the Vrije Universiteit Brussels (VUB) and Hans Vanhove of the Katholieke Universiteit Leuven.

Appendix

Algorithm 1: *Evaluation of MARS model parameters for feature interaction between two ordinary non horizontal planar features*

Identify top and bottom planar features, <**Plane-Top**> and <**Plane-Bottom**> using the Z (depth) co-ordinate of the center of the planes
Set <**Wall Angle Difference**> as the difference in the angles of the normal of <**Plane-Top**>**,** <**Nt**> and normal of <**Plane-Bottom**>**,** <**Nb**> with z-axis
Find outer borders of the selected features as <**Outer-Border-Top**> and <**Outer-Border-Bottom**>
for each Feature <**F**> in selected features {
    for each point vector <**V**> with normal <**Nv**> in <**F**> {
        Create normal plane <**Np**> to <**F**> at the point using three points, i) <**V**>
        ii) <**V**>+<**Nv**>*****m iii) <**Np3**>=$V_x\ \hat{i} + V_y\ \hat{j} + (V_z+n)\ \hat{k}$, where m, n are constants
        Intersect outer border of <**F**> with <**Np**> to find intersection points <**P1**> and <**P2**>
        Sort <**P1**> and <**P2**> by Z co-ordinate to find upper intersection point <**Pu**> and lower intersection point <**Pl**>
        Set Total Vertical Feature Distance = Distance from <**V**> to <**Pu**> + Distance from <**V**> to <**Pl**>
        if plane is <**Plane-Top**> {
            Create normal plane <**Npb**> to <**Plane-Bottom**> at the point <**Pl**> using three points, i) < **Pl** > ii) < **Pl** >+<**Nb**>*****m iii) <**Npb3**>=$Pl_x\ \hat{i} + Pl_y\ \hat{j} + (Pl_z+n)\ \hat{k}$
            Intersect outer border of <**Plane-Bottom**> with <**Npb**> to find intersection points <**P3**> and <**P4**>
            Sort <**P3**> and <**P4**> by Z co-ordinate to find upper intersection point <**Pbu**> and lower intersection point <**Pbl**>
            Set Vertical Combined Feature Distance = Distance from <**V**> to <**Pl**> + Distance from <**Pl**> to <**Pbl**>
            Set Total Vertical Combined Feature Length = Distance from <**V**> to <**Pu**> **+** Vertical Combined Feature Distance
        }

        if plane is <**Plane-Bottom**> {
            Create normal plane <**Npu**> to <**Plane-Top**> at the point < **Pu** > using three points, i) < **Pu** > ii) < **Pu** >+<**Nt**>*****m iii) <**Npu3**>=$Pu_x\ \hat{i} + Pu_y\ \hat{j} + (Pu_z+n)\ \hat{k}$
            Intersect outer border of <**Plane-Top**> with <**Npu**> to find intersection points <**P5**> and <**P6**>
            Sort <**P5**> and <**P6**> by Z co-ordinate to find upper intersection point <**Ptu**> and lower intersection point <**Ptl**>
            Set Vertical Combined Feature Distance = Distance from <**V**> to <**Pl**>
            Set Total Vertical Combined Feature Length = Distance from <**V**> to <**Pu**> **+** Vertical Combined Feature Distance + Distance from <**Pu**> to <**Ptu**>
        }
}

References

[1] Jeswiet J, Micari F, Hirt G, Bramley A, Duflou JR, Allwood J. Asymmetric single point incremental forming of sheet metal. CIRP Annals Manufacturing Technology 2005; 54(2):623-649

[2] Rauch M, Hascoet J, Hamann J, Plenel Y. Tool path programming optimization for incremental sheet forming applications. Computer-Aided Design 2009; 41:877-885

[3] Ambrogio G, Costantino I, Napoli L, Filice L, Fratini L, Muzzupappa M. Influence of some relevant process parameters on the dimensional accuracy in incremental forming: a numerical and experimental investigation. Journal of Materials Processing Technology 2004; 153–154:501–507

[4] Skjoedt M, Hancock MH, Bay N. Creating Helical Tool Paths for Single Point Incremental Forming. Key Engineering Materials 2007; 344:583-590

[5] Micari F, Ambrogio G, Filice L. Shape and dimensional accuracy in Single Point Incremental Forming: State of the art and future trends. Journal of Materials Processing Technology 2007; 191: 390–395

[6] Bambach M, Taleb Araghi B, Hirt G. Strategies to improve the geometric accuracy in asymmetric single point incremental forming. Production Engineering - Research and Development (2009); 3:145–156

[7] Verbert J, Duflou JR, Lauwers B. Feature Based Approach for Increasing the Accuracy of the SPIF Process. Key Engineering Materials 2007; 344:527-534

[8] Duflou JR, Lauwers B, Verbert J, Tunckol Y, Baerdemaeker HD. Achievable Accuracy in Single Point Incremental Forming: Case Studies. Proceedings of the 8th Esaform conference on material forming. 2005; 2:675-678

[9] Hirt G, Ames J, Bambach M, Kopp R. Forming strategies and Process modelling for CNC Incremental sheet forming. Annals of the CIRP. 2004; 53(1):203-206.

[10] Behera AK, Vanhove H, Lauwers B, Duflou JR. Accuracy Improvement in Single Point Incremental Forming Through Systematic Study of Feature Interactions. Key Engineering Materials 2011; 473: 881-888

[11] Ambrogio G, Cozza V, Filice L, Micari F. An analytical model for improving precision in single point incremental forming. Journal of Materials Processing Technology. 2007; 191:92–95

[12] He S, Van Bael A, Van Houtte P, Duflou JR, Szekeres A, Henrard C, Habraken AM. Finite Element Modeling of Incremental Forming of Aluminum Sheets. Advanced Materials Research. 2005; 6-8:525-532

[13] Henrard C, Bouffioux C, Duchêne L, Duflou JR, Habraken AM. Validation of a New Finite Element for Incremental Forming Simulation Using a Dynamic Explicit Approach. Key Engineering Materials. 2007; 344:495-502

[14] Hadoush, A, van den Boogaard, AH. Efficient Implicit Simulation of Incremental Sheet Forming. International Journal for Numerical Methods in Engineering. 2011;doi: 10.1002/nme.3334

[15] Verbert J, Behera AK, Lauwers B, Duflou JR. Multivariate Adaptive Regression Splines as a Tool to Improve the Accuracy of Parts Produced by FSPIF. Key Engineering Materials. 2011; 473:841-846

[16] Lefebvre P, Lauwers B. Multi-axis machining operation evaluation for complex shaped part features. Proceedings of 4th CIRP ICME International Seminar on Intelligent computation in Manufacturing Engineering. 2004; 345-350

[17] Jiao X, Heath MT. Feature detection for surface meshes. Proceedings of the 8th International Conference on Grid Generation in Computational Field Simulations. 2002:705-714.

[18] Chua CK, Leong KF, Lim CS. Rapid prototyping: principles and applications. World Scientific. 2nd Edition. 2003

[19] Varady T, Martin RR, Coxt J. Reverse engineering of geometric models - an introduction, Computer Aided Design. 1997:255-268

[20] Leathwick JR, Rowe D, Richardson J, Elith J, Hastie T. Using multivariate adaptive regression splines to predict the distributions of New Zealand's freshwater diadromous fish. Freshwater Biology. 2005; 50:2034–2052

[21] R Development Core Team. R: A Language and Environment for Statistical Computing. R Foundation for Statistical Computing. 2004.

[22] Hastie T, Tibshirani RJ, Friedman JH. The Elements of Statistical Learning: Data Mining, Inference and Prediction. Springer-Verlag, New York. 2001.

[23] Bentley JL. Multidimensional binary search trees used for associative searching. Communications of Association for Computing Machinery (ACM). 1975; 18:509–517.

[24] Bentley JL. K-d trees for semidynamic point sets. Proceedings of the 6th Annual Symposium on Computational Geometry. 1990:187–197.

[25] Duflou JR, Verbert J, Belkassem B, Gu J, Sol H, Henrard C, Habraken, AM. Process window enhancement for single point incremental forming through multi-step toolpaths. CIRP Annals-Manufacturing Technology. 2008; 57(1):253-256

Vitae

Amar Kumar Behera is an international research scholar at Katholieke Universiteit Leuven. He received his B.Tech., M.Tech. and Minor degrees from the Indian Institute of Technology, Kharagpur in 2005 and MSME degree from the University of Illinois at Urbana-Champaign in 2008. His research interests include geometric algorithms in CAD/CAM, rapid prototyping, sheet metal forming and systems modeling and simulation.

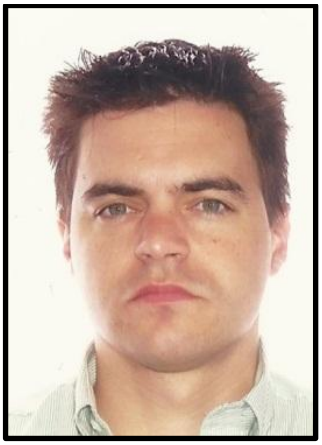

Johan Verbert was a research scholar at the Department of Mechanical Engineering, Katholieke Universiteit Leuven. He obtained his Master of Science in Computer Science Engineering degree in 2004 and a PhD in Engineering in 2010 from KU Leuven. His interests include CAD/CAM, software engineering, incremental sheet metal forming and process control. He currently works in the private sector, in the field of thermoforming.

Bert Lauwers is a full professor at the Department of Mechanical Engineering, Katholieke Universiteit Leuven. A fellow of CIRP, he received his PhD degree in engineering in 1993 from KU Leuven. His research interests are in the areas of manufacturing processes (multi-axis milling, high

speed machining, electrical discharge machining, ultrasonic assisted machining, hybrid processes) and computer support in manufacturing such as CAD/CAM, NC-programming and digital manufacturing.

Joost R. Duflou is a full professor at the Department of Mechanical Engineering, Katholieke Universiteit Leuven. He holds master degrees in architectural and electro-mechanical engineering. and a PhD in engineering from the KU Leuven, Belgium. His principal research activities are situated in the fields of sheet metal forming, design support methods and methodologies, systematic innovation, project management and life cycle engineering. He is a member of CIRP and has published over 200 international publications.